Unraveling the Dynamics of the $C(^3P,^1D) + C_2H_2$ Reactions by the Crossed Molecular Beam Scattering Technique†

Francesca Leonori, Raffaele Petrucci, Enrico Segoloni, Astrid Bergeat,‡ Kevin M. Hickson, Nadia Balucani, and Piergiorgio Casavecchia*

Dipartimento di Chimica, Università degli Studi di Perugia, 06123 Perugia, Italy

Received: September 21, 2007; In Final Form: December 3, 2007

A detailed investigation of the dynamics of the reactions of ground- and excited-state carbon atoms, $C(^3P)$ and $C(^1D)$, with acetylene is reported over a wide collision energy range (3.6−49.1 kJ mol^{-1}) using the crossed molecular beam (CMB) scattering technique with electron ionization mass spectrometric detection and time-of-flight (TOF) analysis. We have exploited the capability of (a) generating continuous intense supersonic beams of $C(^3P, ^1D)$, (b) crossing the two reactant beams at different intersection angles (45, 90, and 135°) to attain a wide range of collision energies, and (c) tuning the energy of the ionizing electrons to low values (soft ionization) to suppress interferences from dissociative ionization processes. From angular and TOF distribution measurements of products at m/z=37 and 36, the primary reaction products of the $C(^3P)$ and $C(^1D)$ reactions with C_2H_2 have been identified to be cyclic (c)-C_3H + H, linear (l)-C_3H + H, and $C_3 + H_2$. From the data analysis, product angular and translational energy distributions in the center-of-mass (CM) system for both the linear and cyclic C_3H isomers as well as the C_3 product from $C(^3P)$ and for l/c-C_3H and C_3 from $C(^1D)$ have been derived as a function of collision energy from 3.6 to 49.1 kJ mol^{-1}. The cyclic/linear C_3H ratio and the $C_3/(C_3 + c/l\text{-}C_3H)$ branching ratios for the $C(^3P)$ reaction have been determined as a function of collision energy. The present findings have been compared with those from previous CMB studies using pulsed beams; here, a marked contrast is noted in the CM angular distributions for both C_3H- and C_3-forming channels from $C(^3P)$ and their trend with collision energy. Consequently, the interpretation of the reaction dynamics derived in the present work contradicts that previously proposed from the pulsed CMB studies. The results have been discussed in the light of the available theoretical information on the relevant triplet and singlet C_3H_2 ab initio potential energy surfaces (PESs). In particular, the branching ratios for the $C(^3P) + C_2H_2$ reaction have been compared with the available theoretical predictions (approximate quantum scattering calculations and quasiclassical trajectory calculations on ab initio triplet PESs and, very recent, statistical calculations on ab initio triplet PESs as well as on ab initio triplet/singlet PESs including nonadiabatic effects, that is, intersystem crossing). While the experimental branching ratios have been corroborated by the statistical predictions, strong disagreement has been found with the results of the dynamical calculations. The astrophysical implications of the present results have been noted.

I. Introduction

The reaction of ground-state carbon atoms, $C(^3P)$, with acetylene exhibits three competing, thermodynamically accessible channels

$$C(^3P) + C_2H_2(X^1\Sigma_g^+) \rightarrow l\text{-}C_3H(X^2\Pi_{1/2}) + H(^2S_{1/2}) \quad \Delta H^\circ_0 = -1.5 \text{ kJ mol}^{-1} \quad (1a)$$

$$\rightarrow c\text{-}C_3H(X^2B_2) + H(^2S_{1/2}) \quad \Delta H^\circ_0 = -8.8 \text{ kJ mol}^{-1} \quad (1b)$$

$$\rightarrow C_3(X^1\Sigma_g^+) + H_2(X^1\Sigma_g^+) \quad \Delta H^\circ_0 = -106 \pm 16 \text{ kJ mol}^{-1} \quad (1c)$$

Channel 1c is spin-forbidden, however, and can only take place via intersystem crossing (ISC) from triplet to singlet C_3H_2 potential energy surfaces (PESs). The indicated exoergicities for channels 1a and 1b are those obtained by Ochsenfeld et al.[1] by high-quality ab initio calculations of reaction intermediates and products (estimated uncertainties are about ±4−5 kJ mol^{-1}), while that for channel 1c is taken from literature data on the heats of formation (see section IV.3). Reaction 1 can be seen as a prototype of a host of reactions of C atoms with alkynes, which are efficient pathways for the production of long carbon chain molecules both in the interstellar medium (ISM)[2] and in combustion systems.[3,4] Notably, both l-C_3H and c-C_3H have been observed by radioastronomy in a range of interstellar environments, including both cold, dense interstellar clouds (ISCs)[5] and warmer translucent clouds.[6] C_3 has also been detected both in circumstellar envelopes[7−9] and ISCs,[9] as well as in comets (see section V).

The corresponding reactions of excited-state carbon atoms $C(^1D)$ are

† Originally submitted for the "Giacinto Scoles Festschrift", published as the December 13, 2007 issue of *J. Phys. Chem. A* (Vol. 111, No. 49).

* To whom correspondence should be addressed. E-mail: piero@dyn.unipg.it.

‡ Visiting scientist from Institut des Sciences Moléculaires, UMR 5255 CNRS-Université Bordeaux 1, 33405 Talence Cedex, France.

10.1021/jp0776208 CCC: $40.75
Published on Web 01/30/2008

$$C(^1D) + C_2H_2(X^1\Sigma_g^+) \rightarrow l\text{-}C_3H(X^2\Pi_{1/2}) + H(^2S_{1/2})$$
$$\Delta H^\circ_0 = -123.4 \text{ kJ mol}^{-1} \quad (2a)$$

$$\rightarrow c\text{-}C_3H(X^2B_2) + H(^2S_{1/2})$$
$$\Delta H^\circ_0 = -130.5 \text{ kJ mol}^{-1} \quad (2b)$$

$$\rightarrow C_3(X^1\Sigma_g^+) + H_2(X^1\Sigma_g^+)$$
$$\Delta H^\circ_0 = -228 \pm 16 \text{ kJ mol}^{-1} \quad (2c)$$

Here, for the l/c-C_3H-forming channels, the reaction enthalpies are obtained by adding the ($^1D-^3P$) energy splitting (121.9 kJ mol^{-1}) to the enthalpies[1] for the corresponding C(^3P) reactions.

Reaction 1 has been studied extensively over the past 10 years both experimentally and theoretically. Kinetic studies at room temperature of a variety of C(^3P) reactions with unsaturated hydrocarbons, including acetylene, found them to be very fast ($k \sim 2-3 \times 10^{-10}$ cm^3 molecule^{-1} s^{-1}), suggesting that they are barrierless processes dominated by long- range attractive forces.[10] Novel kinetic measurements down to 15 K demonstrated that these reactions are very fast ($k \sim 4 \times 10^{-10}$ cm^3 molecule^{-1} s^{-1}) even at this very low temperature[11] and hence confirmed the earlier hypothesis. Dynamics experiments,[12−20] in addition to theoretical studies,[1,21−26] were able to provide information on the primary products and their relative importance as a function of collision energy. Figure 1 depicts schematically the triplet and singlet C_3H_2 PESs as predicted by electronic structure calculations.[1,23,26] It should be noted that all recent ab initio calculations[1,22−26] on the C(^3P) + C_2H_2 reaction agree that the cyclic C_3H isomer is more stable than the linear isomer, but uncertainty still exists on the exoergicity of processes 1a and 1b. Despite the extensive body of earlier work, there is still no consensus on the microscopic mechanism and dynamics for this reaction. In fact, a strong disagreement exists between the results of the experimental dynamical studies,[1,12−14,17−20] as well as between the results of the theoretical dynamical investigations.[24−26]

A brief summary of previous dynamical work is given here to remark on the most significant discrepancies. A first CMB study at three collision energies, E_c (8.8, 28.0, and 45.2 kJ mol^{-1}), complemented by ab initio calculations of the relevant triplet C_3H_2 PES, was published by Kaiser et al.[1,12−14] This CMB study, which used pulsed C(^3P) beams obtained by laser ablation of graphite and a continuous C_2H_2 beam, identified C_3H + H as the sole reaction channel. It was concluded that the spin-forbidden pathway (1c) was not open in the investigated energy range. The linear and cyclic C_3H isomer contributions were not resolved in the experiments, and the data analysis was carried out in terms of a single set of center-of-mass (CM) product angular, $T(\theta)$, and translational energy, $P(E'_T)$, distributions. Nevertheless, on the basis of the C_3H product $T(\theta)$, Kaiser et al.[12−14] inferred the formation of c-C_3H and l-C_3H isomers via direct and indirect, respectively, scattering dynamics, with c-C_3H being preferentially formed at low E_c and becoming negligible at high E_c. Later, Kaiser et al.[27] also published a CMB study on the dynamics of reaction 2, exploiting the fact that by selecting the fast part of the laser-ablated carbon beam, C(^1D) could be produced almost exclusively. The $m/z = 36$ and 37 time-of-flight (TOF) and angular distributions were reported to show identical patterns, indicating that the C_3 + H_2 channel (which is spin-allowed for C(^1D)) was absent within their detection limits.

In our laboratory, we initiated an investigation of C atom reactions with unsaturated hydrocarbons using the CMB technique with continuous beams.[16,28] The title reactions were studied at $E_c = 29.3$ kJ mol^{-1} using a continuous carbon atom beam containing both C(^3P) and excited C(^1D) (in a significant percentage), and it was clearly demonstrated that, in addition to the H-elimination channel (channels 1a and 1b), the H_2 elimination pathway (channel 1c) leading to $C_3(X^1\Sigma_g^+)$ + $H_2(X^1\Sigma_g^+)$ also plays an important role.[16] A synergic study of differential and integral reactive cross sections for the C(^3P) + C_2H_2 reaction was then published in collaboration with the Bordeaux group.[17,18] The derived $T(\theta)$ of the C_3H product at $E_c = 29.3$ kJ mol^{-1} was interpreted as arising from a reaction occurring through an intermediate long-lived complex[29] whose lifetime is on the order of a few rotational periods. The branching ratio of cross sections in the C(^3P) reaction, $\sigma(C_3 + H_2)/[\sigma(C_3 + H_2) + \sigma(C_3H + H)]$, was determined to be 0.37. This result was found to be consistent with that of a complementary investigation[30] of the detailed kinetics of C(^3P) + C_2H_2 at 300 K, which found an upper limit for the branching ratio of H production, that is, $k_{(1a+1b)}/k_1$, of only 0.53 ± 0.04, thus suggesting that pathway 1c could account for the rest (that is, $k_{1c}/k_1 = 0.47 \pm 0.04$). At that time, no information could be obtained about the respective weights of pathways 1a and 1b. In addition, we derived information on the dynamics of formation of C_3H from C(^1D) + C_2H_2 (reaction 2a,b) at the same E_c.[17] In 2001, Kaiser et al.[31] reported the preliminary results of a reinvestigation of the C(^3P) + C_2H_2 reaction at E_c = 16.6 kJ mol^{-1} using two pulsed beams of the reagents in which, due to an improvement in the signal-to-noise ratio (S/N) with respect to the previous studies,[12−14] they observed that the $m/z = 36$ signal actually originates from two different channels and thus confirmed the occurrence of the C_3 + H_2 channel.

The above experimental studies triggered several theoretical studies, mainly aimed at predicting the branching ratio between c-C_3H and l-C_3H from the C(^3P) reaction as a function of E_c. Buonomo and Clary[24] developed a reduced-dimensionality model for generation of the PES and, using time-dependent wave packet calculations to obtain reaction probabilities, provided information about the ratio of cross sections for c-C_3H and l-C_3H formation, $\sigma_{cyclic}/\sigma_{linear}$. The l-$C_3H$ was found to be overwhelmingly formed at the lowest collision energy sampled, $\sigma_{cyclic}/\sigma_{linear} < 0.02$ at $E_c = 5$ kJ mol^{-1}, with c-C_3H formation augmenting gradually to reach a plateau, $\sigma_{cyclic}/\sigma_{linear} = \sim 0.17$ between E_c = 50 and 70 kJ mol^{-1}. These results were in disagreement with the conclusion of Kaiser et al.[12−14] Another theoretical study was more recently performed by Takayanagi[25] with a model in three degrees of freedom treating the C + C_2H_2 reaction as a standard atom−diatom system; results completely contradictory to those of Buonomo and Clary[24] were obtained from approximate quantum scattering calculations, with $\sigma_{cyclic}/\sigma_{linear} > 10^2-10^4$ between $E_c = 0.1$ and 58 kJ mol^{-1}.

In view of these discrepant results, it was clear that the detailed dynamics of the C(^3P) + C_2H_2 reaction were still unresolved and that more precise theoretical and experimental work was required to determine the exoergicity of the l-C_3H + H and c-C_3H + H pathways as well as for the evaluation of the dynamics of l-C_3H, c-C_3H, and C_3 formation and branching ratios as a function of E_c. To address these issues, in our laboratory, we took advantage of the novel variable beam crossing angle setup and studied the reaction at $E_c = 3.5$ and 18.5 kJ mol^{-1}, achieved by crossing the two reactant beams at 45° and seeding the C beam in Ne and He, respectively.[19] The study[19] was performed in synergistic fashion with pulsed CMB experiments in Bordeaux using VUV H-atom detection within

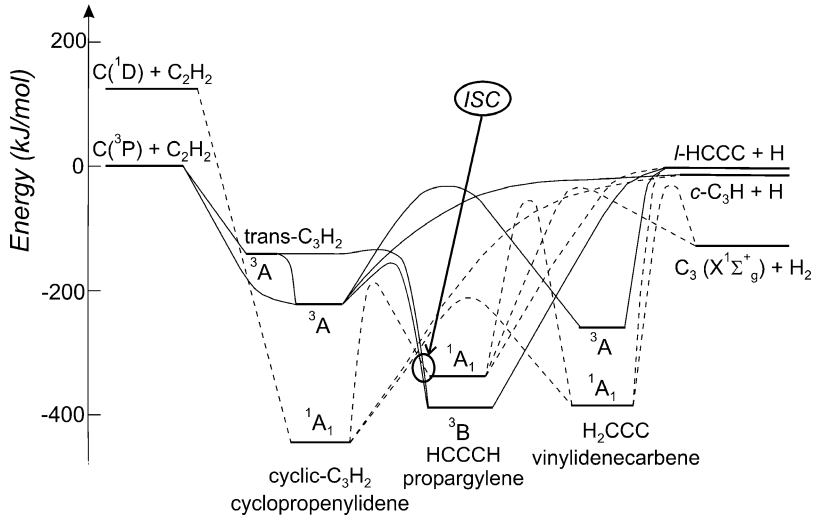

Figure 1. Schematic representation of the triplet and singlet C_3H_2 potential energy surfaces (adapted from refs 1, 21, 22, 23, 26, and 32). The energetic is taken from ref 32. The triplet−singlet seam of intersystem crossing (see refs 23 and 32) is labeled with ISC.

a Doppler scheme, down to $E_c = 0.8$ kJ mol^{-1}. Although the data analysis at $E_c = 3.5$ and 18.5 kJ mol^{-1} permitted us to derive also the reaction dynamics of the $C(^1D)$ reaction, DCSs in the CM system were reported and discussed only for the $C(^3P)$ reaction (channels 1a−c). The two main reaction pathways leading to H and H_2 elimination were unambiguously disentangled from differences in the $m/z = 37$ and 36 angular distributions (Figures 4 and 5, respectively, of ref 19) and the observation of distinct features in the TOF measurements at $m/z = 36$ (see Figure 6 in ref 19). Because of the high S/N in the angular distribution data at $m/z = 37$, measured at every degree in the laboratory (LAB) frame, and by exploiting the theoretical information[1] on the relative exoergicity of the linear and cyclic channels (1a and b), it has been possible to derive CM angular and translational energy distributions for the c-C_3H + H and l-C_3H + H forming channels, as well as for $C_3 + H_2$, and determine their branching ratios. At both E_c's, the formation of c-C_3H, l-C_3H, and C_3 from $C(^3P)$ was found to be characterized by a backward−forward symmetric $T(\theta)$, which indicates that all three channels (1a−c) proceed through the formation of long-lived C_3H_2 complexes, that is, complexes whose lifetimes are of many (>5) rotational periods.[29] This is corroborated by statistical calculations of the various possible C_3H_2 complexes on ab initio PESs that found their lifetimes to be on the order of tens of picoseconds to nanoseconds at 300 K.[22] Our results[19] were found to be in strong disagreement with those reported previously by Kaiser et al.[12−14] for the $C_3H + H$ channel. The ratios of cross sections $\sigma_{cyclic}/\sigma_{linear}$ as a function of E_c were also obtained.[19] The experimental results indicated that c-C_3H is preferentially formed at low E_c. The ratio $\sigma_{cyclic}/\sigma_{linear}$ was found to decrease with increasing E_c, from ∼9 at $E_c = 0.8$ kJ mol^{-1} to ∼3.4 at $E_c = 3.5$ kJ mol^{-1} and ∼1.6 at $E_c = 18.5$ kJ mol^{-1}. These results contradict both quantum scattering studies by Buonomo and Clary[24] and by Takayanagi.[25] In addition, from the extent of the $P(E'_T)$ functions for l- and c-C_3H, we were able to derive an improved exoergicity for channel 1b; the latter was found to be ∼2.5 kJ mol^{-1} larger than the theoretical value[1] of 8.6 kJ mol^{-1} and was corroborated by the Bordeaux measurements at $E_c = 0.8$ kJ mol^{-1}.[19]

In 2006, Bowman and co-workers[26] reported a full-dimensional density functional theory (DFT) study of the C_3H_2 triplet and singlet PESs and used these surfaces in QCT calculations of the $C(^3P) + C_2H_2$ reaction dynamics. The calculations on the triplet PES found both l-C_3H and c-C_3H products, with l-C_3H being dominant in the energy range considered (5−40 kJ mol^{-1}). These results are consistent with the finding of Buonomo and Clary,[24] while they are opposite to those of Takayanagi;[25] however, they are also in disagreement with our recent experimental findings.[19] Limited calculations of unimolecular reaction dynamics on the singlet PES found both C_3H isomeric products to be generated in comparable amounts from the $C(^1D) + C_2H_2$ reaction in addition to the $C_3 + H_2$ products.[26]

Very recently, Kaiser and co-workers[20] have reinvestigated the dynamics of the $C(^3P) + C_2H_2$ reaction by performing new CMB experiments with pulsed beams using a new apparatus with improved S/N at three different E_c's (8.0, 20.4, and 30.7 kJ mol^{-1}). These studies were supplemented by experiments using three isotopomers, C_2D_2, C_2HD, and $^{13}C_2H_2$, because the presence of large concentrations of C_2 and C_3 in the carbon beam represents a complication in those studies. Specifically, the reaction $C_2 + C_2H_2$ produces C_4H as the main product, which fragments heavily under electron ionization to C_3H^+ ($m/z = 37$). Furthermore, C_3 elastically scattered from the C_2H_2 beam gives a very large contribution to the $m/z = 36$ signal at small angles (close to the C beam). Despite these problems, the former complication could be disentangled in the data analysis through TOF measurements, and the latter was overcome by using $^{13}C_2H_2$.[20] Notably, the dynamics of formation of $C_3H + H$ was confirmed to be identical to that derived in the previous experiments,[12−14] and therefore, they remain in strong contrast with our results.[19] In this reinvestigation,[20] the dynamics of formation of $C_3 + H_2$ were also derived.

Finally, Mebel et al.[32] very recently combined ab initio CCSD(T) calculations of intermediates and transition states on the singlet and triplet C_3H_2 PESs extrapolated to the complete basis set limit with statistical computations of energy-dependent rate constants of the $C(^3P) + C_2H_2$ reaction under CMB conditions. RRKM theory was applied in this study for isomerization and dissociation steps within the same multiplicity and radiationless transitions, and nonadiabatic transition-state theories were used for singlet−triplet ISC rates. The calculated rate constants were utilized to predict product branching ratios. This detailed study[32] offers the opportunity to compare the branching ratios derived from the previous[17,19] and present experimental work with detailed statistical predictions, which also include nonadiabatic effects. In addition, new accurate exoergicities for channel 1a ($\Delta H°_0 = -3.1 \pm \sim 4$ kJ mol^{-1}) and channel 1b ($\Delta H°_0 = -14.1 \pm \sim 4$ kJ mol^{-1}) are reported;[32]

TABLE 1: Characteristics of the Continuous Supersonic Beams of the Reactants

gas mixture	P (mbar)[a]	v (m s^{-1})[b]	$\Delta v/v$[c]	E_c (kJ mol^{-1})[d]	$\Delta\alpha$ (deg)[e]	beam crossing angle (deg)
			C-Atom Beam			
1.5% CO/0.8% O_2 / Ne	300	1326	0.35	3.6	3	45
1.5% CO/0.8% O_2 / Ne	50	1196	0.36	8.6	3	90
1.5% CO/0.8%O_2 / He	100	2632	0.25	18.6	3	45
1.5% CO/0.8%O_2 / He	210	2838	0.32	49.1	3	135
C_2H_2 beam						
neat	450	828	0.26		7	45
neat	450	823	0.26		7	90
neat	400	810	0.26		7	135

[a] Pressure of the gas mixture in front of the nozzle. Nozzle diameter is 0.26 mm for the He-seeded beam at 135° and the Ne-seeded beam at 45°, while there is a 0.52 mm diameter for the Ne-seeded beam at 90° and the He-seeded beam at 45°. [b] Peak velocity from single-shot TOF measurements. Systematic errors are estimated within 1%. [c] Velocity spread (fwhm). [d] Collision energy obtained when crossed with the C_2H_2 beam. [e] Beam angular divergence (fwhm).

these new values should be more accurate than the previous values[1] ($\Delta H°_0 = -8.6 \pm \sim 4$ and $-1.5 \pm \sim 4$ kJ mol^{-1}, respectively), although they lie within the estimated uncertainties.

In this paper, we report new measurements at two collision energies, $E_c = 8.6$ and 49.1 kJ mol^{-1} (obtained by crossing the two reactants beams at 90° with a C/Ne-seeded beam and at 135° with a C/He-seeded beam, respectively) and a fine-tuning partial reanalysis[33] of the previous data[19] at E_c=3.5 (now 3.6) and 18.5 (now 18.6) kJ mol^{-1}. The new results, together with the recent ones[19] at $E_c = 3.6$ and 18.6 kJ mol^{-1} and the previous ones[17] obtained at $E_c = 29.3$ kJ mol^{-1}, permit us to examine the reaction dynamics of the C(^{3}P) + C_2H_2 reaction in an extended range of collision energies. As the continuous carbon beam contains both (^{3}P,^{1}D) species, the dynamics of the C(^{1}D) reactions (2a−c) have also been characterized. The derived C(^{3}P) and C(^{1}D) reaction dynamics will be discussed in the light of the ab initio triplet and singlet C_3H_2 PESs and compared to those derived from previous[12,13,27] and recent[20] CMB work carried out using pulsed beams. In particular, the branching ratios will be compared with the theoretical predictions from both QCT calculations[26] and reduced dimensionality QM calculations[24,25] on ab initio triplet PESs and from the recent statistical calculations of Mebel et al.[32] A clearer picture of the reaction dynamics as a function of collision energy will be given.

II. Experimental Section

The experiments were performed using a CMB apparatus with mass spectrometric TOF detection,[34,35] which has been recently upgraded.[36−39] First, product detection by the "soft" electron ionization technique, which allows us to limit the dissociative ionization of interfering species, was implemented on the experiment. Second, the accessible range of E_c was extended by adding 45 and 135° beam intersection angle configurations to the previous one at 90°.

Briefly, two continuous supersonic beams of the reactants—collimated in angle and velocity—are crossed at 45, 90, or 135° under single-collision conditions in a large scattering chamber kept at 2×10^{-6} mbar in operating conditions (2×10^{-7} mbar base pressure). The angular and velocity distributions of the reaction products are recorded by a triply differentially pumped, ultrahigh-vacuum (10^{-11} mbar) electron impact ionizer followed by a quadrupole mass filter and particle multiplier. The ionizer features tunable electron energies from 100 eV down to ∼8−9 eV and was typically operated at 25 eV to suppress elastic interferences from the acetylene beam. The whole detector unit can be rotated in the plane of the two beams around their intersection axis. The velocity of the reactants is derived by using the single-shot TOF analysis, while the velocity of the products is obtained by using the pseudo-random TOF technique.[40] In the present work, continuous supersonic beams of C atoms were produced by means of a radio frequency (RF) discharge in a water-cooled quartz nozzle which operated at high RF power (260 W) and relatively high pressure (∼300 (100) mbar with a 0.24 (0.50) mm diameter nozzle) on a dilute (1.5%) mixture of a suitable precursor molecule, CO, in O_2-(0.8%)/He or Ne carrier gases. Atomic carbon was produced mainly in the ground ^{3}P state, but a significant concentration in the excited $^1D_2$ state (lying 121.9 kJ mol^{-1} above the ground state) was also present, as demonstrated by a CMB study of the C(^{1}D) + H_2/D_2 reactions[41−43] and by measurements of electron ionization efficiency curves of the carbon atom beam. The C beam contained only 3−4% C_2 and no detectable C_3 (from mass spectroscopic TOF analysis); this characteristic is particularly important in the present study because C_3 is one of the energetically allowed products of the reaction under study, and the low concentration of C_2 made the contribution of C_3H coming from dissociative ionization of the C_4H product formed from the C_2 + C_2H_2 reaction[44] also negligible (this reaction has been recently studied also in our laboratory[45]). A supersonic beam of acetylene was produced by expanding 0.40 or 0.45 bar of pure gas through a stainless steel nozzle (0.1 mm diameter) kept at room temperature. An acetone/dry ice slush trap (−78 °C) was used on the C_2H_2 gas line to trap acetone impurities. Under these expansion conditions, C_2H_2 clustering was negligible. The various characteristics of the C and C_2H_2 beams and the resulting relative translational energies of the experiments are listed in Table 1.

Product angular distributions at $m/z = 37$ and 36 were recorded by modulating the C_2H_2 beam at 160 Hz for background subtraction and taking at least 4−6 scans at each mass, with a typical 50 s counting time at each angle, sufficient to reduce the uncertainty (1−3%). Product TOF distributions at $m/z = 37$ and 36 were then recorded at selected LAB angles using the pseudo-random TOF technique at 5 μs/channel; typical counting times varied from 10 to 180 min depending on the signal intensity.

The relevant dynamic information, that is, the product flux in the CM frame, $I_{CM}(\theta,u)$, is as usual retrieved using a forward convolution fit of the angular, $N(\Theta)$, and TOF, $N(\Theta, t)$, distributions obtained in the LAB frame. The CM product flux is treated as being separable into an angular part $T(\theta)$ and a velocity part $P(u)$, $I_{CM}(\theta,u) = T(\theta) \times P(u)$, with the latter part generally expressed as a function of the product recoil energy distribution, $P(E'_T)$. The transformation of the CM flux to the LAB number density $N(\Theta)$ is given by $N(\Theta) = (v/u^2)I_{CM}(\theta,u)$.[46]

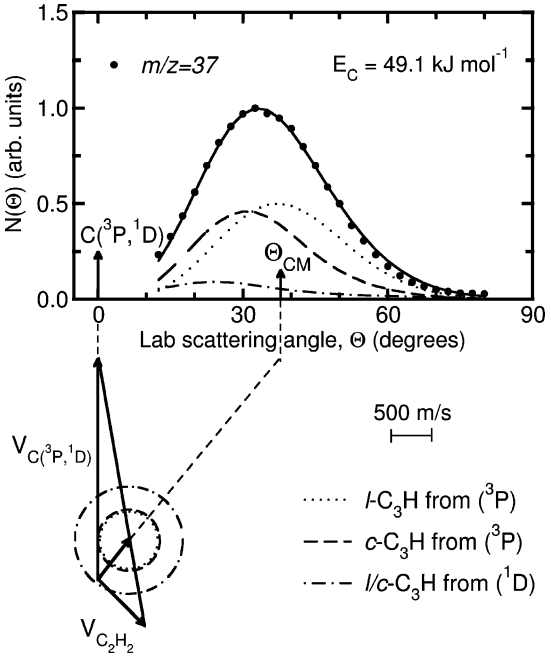

Figure 2. Laboratory angular distribution, $N(\Theta)$ of C_3H products at $m/z = 37$ (solid circles) from the reactions $C(^3P,^1D) + C_2H_2$ at $E_c = 49.1$ kJ mol^{-1}, together with the velocity vector ("Newton") diagram of the experiment. Error bars, when visible outside of the dots, represent ± 1 standard deviation from the mean. The circles in the Newton diagram delimit the maximum velocity that the indicated products (from the reaction of the indicated electronic state of the carbon atom) can attain on the basis of linear momentum and energy conservation if all of the available energy goes into product translational energy. The solid line is the total angular distribution calculated according to eq 3 (see text). The separate contributions of the two possible C_3H isomers from the $C(^3P)$ reactions are indicated with dashed (cyclic isomer) and dotted (linear isomer) lines, while the contribution of c/l-C_3H from the $C(^1D)$ reaction is indicated with a dashed−dotted line.

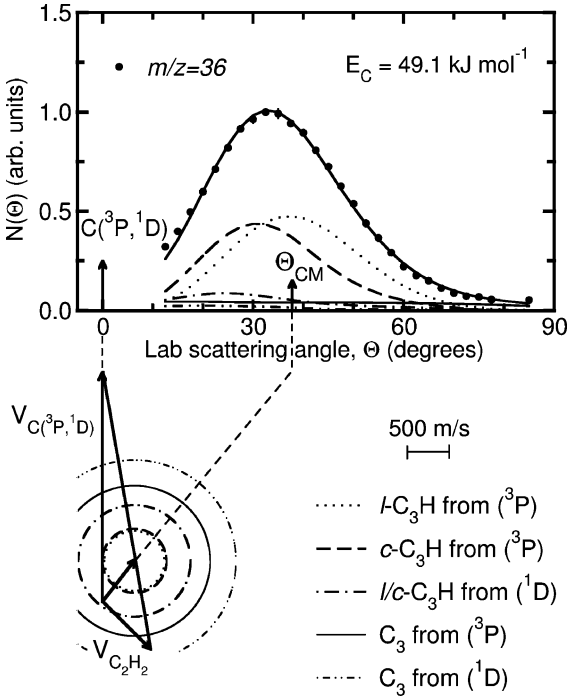

Figure 3. Laboratory angular distribution, $N(\Theta)$, of products at $m/z = 36$ (solid circles) from the reactions $C(^3P,^1D) + C_2H_2$ at $E_c = 49.1$ kJ mol^{-1}, together with the velocity vector ("Newton") diagram of the experiment. Error bars, when visible outside of the dots, represent ± 1 standard deviation from the mean. The circles in the Newton diagram delimit the maximum velocity that the indicated products (from the reaction of the indicated electronic state of the carbon atom) can attain on the basis of linear momentum and energy conservation if all of the available energy goes into product translational energy. The solid line is the total angular distribution calculated according to eq 4 (see text). The separate contributions of the two possible C_3H isomers and C_3 from the $C(^3P)$ reactions are indicated with dashed (cyclic C_3H isomer), dotted (linear C_3H isomer), and light solid (C_3) lines, while the contributions of c/l-C_3H and C_3 from the $C(^1D)$ reactions are indicated with dashed−dotted line (C_3H) and dashed−double dotted lines (C_3).

Simulated LAB densities are calculated by taking into account this transformation and the averaging over experimental parameters, including the energy dependence of the integral reactive cross section, which was taken to vary as $E^{-1/3}$, that is, the typical behavior for barrierless reactions dominated by long-range attractive forces.[47] Simulations obtained using the energy dependence $E^{-0.8}$ measured by Costes et al.[15,17] for E_c below 10 kJ mol^{-1} showed very small differences; only at $E_c = 49.1$ kJ mol^{-1} were the differences significant; however, use of the $E^{-0.8}$ energy dependence at high E_c is not warranted because it has been derived only from experiments at low E_c. The approximation is made that all reaction channels (1a−c and 2a−c) exhibit the same energy dependence of the integral reactive cross section; this appears reasonable because all of the PESs of these processes have similar long-range behavior. The procedure is repeated until a satisfying fit of the experimental LAB densities, $N(\Theta)$ and $N(\Theta, t)$, is achieved and the CM functions, $T(\theta)$ and $P(E'_T)$, so determined are the best-fit functions. In the present study, for the analysis of the distributions at various m/z values, a weighted total $I_{CM}(\theta,E'_T)$ was used, reflecting the contributions of the various possible reaction channels, as described in section III.2.

III. Results and Analysis

III.1. Laboratory Angular and TOF Distributions. Figures 2 and 3 show the $m/z = 37$ and 36 LAB angular distributions, respectively, together with the canonical Newton (that is, velocity vector) diagrams of the experiments for $E_c = 49.1$ kJ mol^{-1}. Error bars, when visible outside of the experimental dots, represent a single standard deviation from the mean. The signal at $m/z = 37$ corresponds only to C_3H products, while that at $m/z = 36$ can originate from direct ionization of C_3 products as well as from dissociative ionization of C_3H products. The dotted and dashed circles in the Newton diagram of Figure 2 delimit the maximum velocity that the l-C_3H and c-C_3H isomer products, respectively, from the $C(^3P)$ reaction can attain if all of the total available energy, $E_{tot} = -\Delta H°_0 + E_c$, goes into product relative translational motion; the dashed−dotted line delimits the maximum velocity of l/c-C_3H formed from the $C(^1D)$ reaction (because of the very small energy difference in the stability of the two isomers with respect to the total energy, a single circle is used to display them in the figure; for the same reason no attempt has been made to disentangle them in the data analysis; see below). The Newton diagram of Figure 3 exhibits two additional circles which, as indicated, delimit the maximum velocity that the C_3 product from the $C(^3P)$ and $C(^1D)$ reactions can attain. As can be seen, the $m/z = 37$ angular distribution features an intense broad peak centered around the CM angle (but slightly displaced in the forward direction with respect to the direction of the C atom) that reflects mainly C_3H products from the weakly exoergic $C(^3P)$ reactions 1a and b and wings (visible only at large angles) of lower intensity which reflect C_3H products from $C(^1D)$ that can be scattered over a much wider angular range because of the much larger exoergicity of the excited C atom reactions 2a and b with respect to

those of ground-state C atoms. In contrast, the $m/z = 36$ angular distribution exhibits wings (visible only at large angles) with a somewhat higher intensity and extending over a wider angular range than those at $m/z = 37$, in addition to an intense peak centered around the CM angle, which reflects C_3H products giving signal at $m/z = 36$ via dissociative ionization. The wings reflect a signal from C_3 originating from both $C(^3P)$ and $C(^1D)$ reactions, that is, pathways 1c and 2c.

Figure 4 shows, for comparison, the TOF spectra recorded at $m/z = 37$ (lhs) and 36 (rhs) at nine LAB angles. The $m/z = 37$ spectra are essentially unstructured and relatively slow, reflecting contribution from the two C_3H isomer channels from $C(^3P)$, which are weakly exoergic and therefore confined in a narrow Newton circle around the CM. The $m/z = 37$ spectra are, however, relatively broad, and this reflects contribution from also l/c-C_3H from $C(^1D)$, which is expected to be significantly faster because channels 2a and b are much more exoergic than channels 1a and b. In contrast, the $m/z = 36$ spectra exhibit, in addition to the same main peak structure as that seen at $m/z = 37$ and now coming from dissociative ionization of C_3H products, also a well pronounced, faster shoulder which is unambiguously attributed, on the basis of energy and linear momentum conservation, to C_3 products from the strongly exoergic $C_3 + H_2$ channels 1c and 2c. Here, we have taken advantage of the higher TOF resolution afforded by the 135° crossing beam configuration. The quality of the experimental results at this high E_c well exemplifies the current capabilities of our improved CMB instrument with a variable beam intersection angle.

Measurements of the $m/z = 37$ product angular and TOF distributions at $E_c = 8.6$ kJ mol^{-1} are shown in Figures 5 and 6, respectively. At this E_c (corresponding to the lowest E_c studied by Kaiser et al.[12,20]), the focus was mainly to characterize the l/c-C_3H-forming channels; therefore, no data were collected at $m/z = 36$, and hence, the dynamics of C_3 formation at this intermediate E_c have not been derived.

III.2. The c/l-C_3H + H Channels. In order to reproduce quantitatively the shape of the angular and TOF distributions at $m/z = 37$, a weighted total CM differential cross section, $I_{CM}(\theta,E'_T)$, reflecting the various possible contributions was used in the data analysis

$$I_{CM}(\theta,E'_T) = w_1 \times [T(\theta)^{3P} \times P(E'_T)^{3P}]_{c-C_3H} + w_2 \times [T(\theta)^{3P} \times P(E'_T)^{3P}]_{l-C_3H} + w_3 \times [T(\theta)^{1D} \times P(E'_T)^{1D}]_{l/c-C_3H} \quad (3)$$

with the parameters w_1 and w_2 representing the relative contribution of cyclic and linear C_3H products, respectively, from the $C(^3P)$ reaction, and w_3 that of l/c-C_3H from the $C(^1D)$ reaction. The dotted, dashed, and dashed−dotted lines in Figures 2 and 5 and 4(lhs) and 6 are the LAB angular and TOF distributions, respectively, generated by the best-fit product angular, $T(\theta)$, and translational energy, $P(E'_T)$, distributions for the $C(^3P)$ and $C(^1D)$ reactions 1a and b and 2a and b, respectively, depicted in Figures 7(lhs) and 8(lhs) for $C(^3P)$ and in Figure 9(lhs) and 10(lhs) for $C(^1D)$. In Figures 7−10, the best-fit functions at $E_c = 3.6$ and 18.6 kJ mol^{-1}, as obtained in our previous work[19] and slightly revised here,[33] are also shown for comparison. The solid lines in Figures 2, 4(lhs), 5, and 6 represent the global best fit according to eq 3 with $w_1 = 0.42$, $w_2 = 0.42$, and $w_3 = 0.16$ for $E_c = 49.1$ kJ mol^{-1} and with $w_1 = 0.39$, $w_2 = 0.19$, and $w_3 = 0.42$ for $E_c = 8.6$ kJ mol^{-1}. It should be noted that the w_i coefficients represent the product of the ith relative reaction cross section multiplied by the

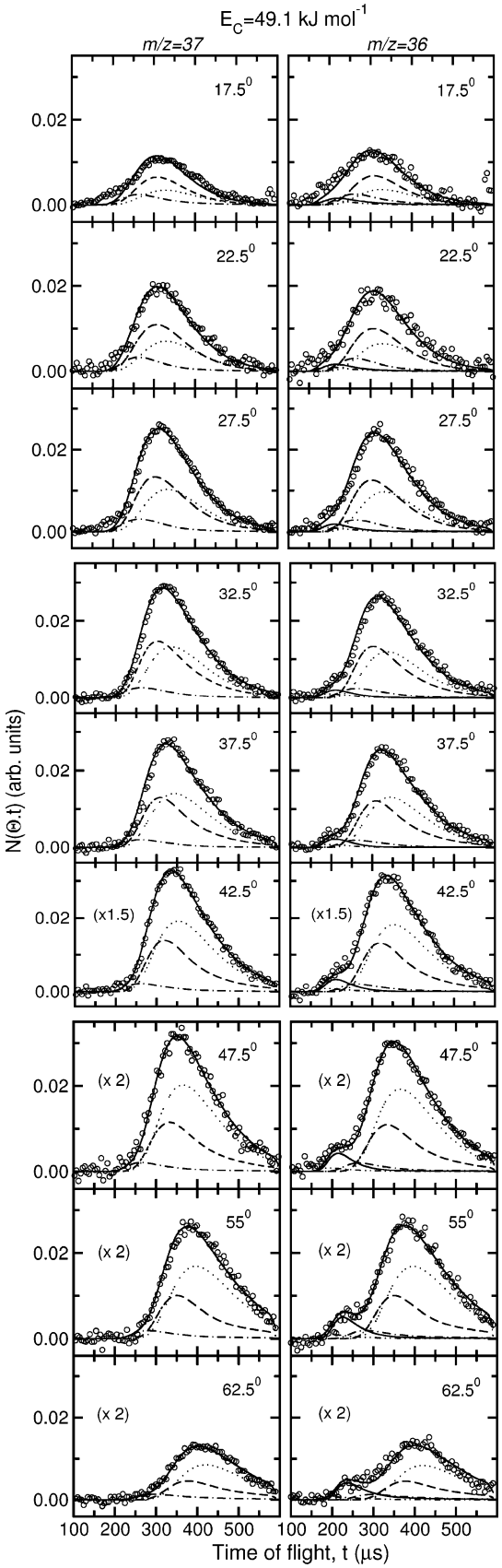

Figure 4. Time-of-flight distributions of the $m/z = 37$ (lhs) and 36 (rhs) products (open circles) for the reactions $C(^3P,^1D) + C_2H_2$ at $E_c = 49.1$ kJ mol^{-1} at the indicated LAB angles. Symbols are as those in Figures 2 and 3. The area of each spectrum at a given angle is equal to the corresponding $N(\Theta)$ intensity at that angle (see Figures 2 and 3); spectra at large angles are multiplied by the indicated factor for display purposes.

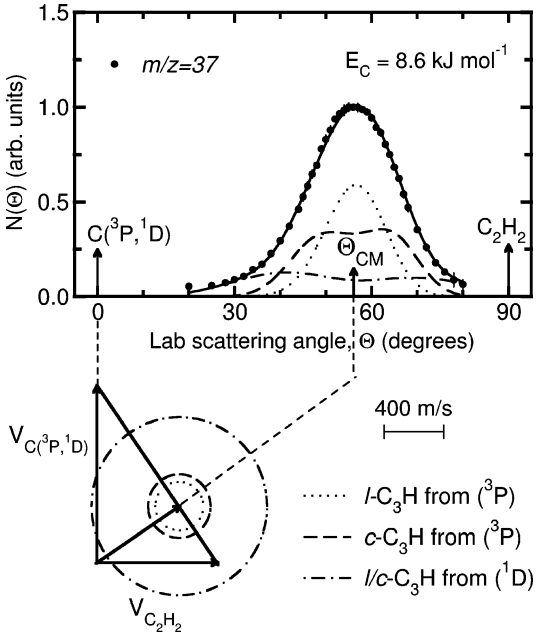

Figure 5. As in Figure 3 but at $E_c = 8.6$ kJ mol^{-1}.

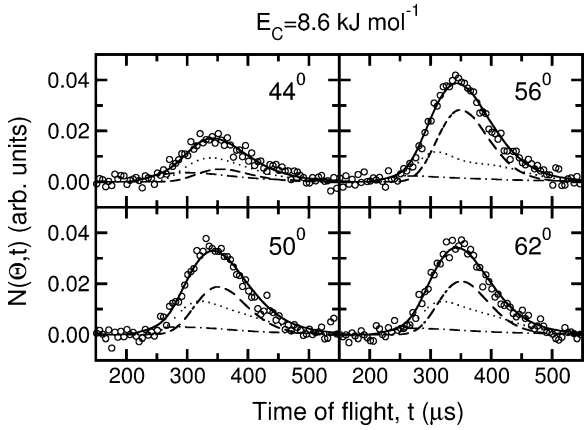

Figure 6. Time-of-flight distributions of the $m/z = 37$ product (open circles) for the reactions $C(^3P,^1D) + C_2H_2$ at $E_c = 8.6$ kJ mol^{-1} at the indicated LAB angles. Symbols are as those in Figure 5. The area of each spectrum is equal to the corresponding $N(\Theta)$ intensity at that angle (see Figure 5).

fractional abundance of $C(^3P)$ or $C(^1D)$ in the beam. The relative abundances of $C(^3P)$ and $C(^1D)$ have not been determined. A rough estimate can be done by assuming that the reactive cross sections for C_3H formation from $C(^3P)$ and $C(^1D)$ are the same and that similar fragmentation patterns hold for C_3H products with somewhat different internal energy content; then, the ratio $w_3/(w_1 + w_2)$ corresponds to the concentration ratio $C(^1D)/C(^3P)$ in the beam. This points to a lower concentration of $C(^1D)$ in the He-seeded beams, especially when small nozzle diameters are used.

It can be noted that the fast part of the $m/z = 37$ TOF spectra (Figure 4(lhs)) and the forward part of the $m/z = 37$ LAB angular distribution (Figure 2) are due to the c-C_3H product, which exhibits a significantly forward scattered $T(\theta)$ (see Figure 7(lhs)) and a $P(E'_T)$ peaking away from zero and extending to 60 kJ mol^{-1} (see Figure 8(lhs)). In contrast, the l-C_3H product, characterized by an isotropic $T(\theta)$ and a $P(E'_T)$ peaking at very low energies, gives a LAB angular distribution centered at the CM angle and TOF spectra peaked at the velocity of the center-of-mass.

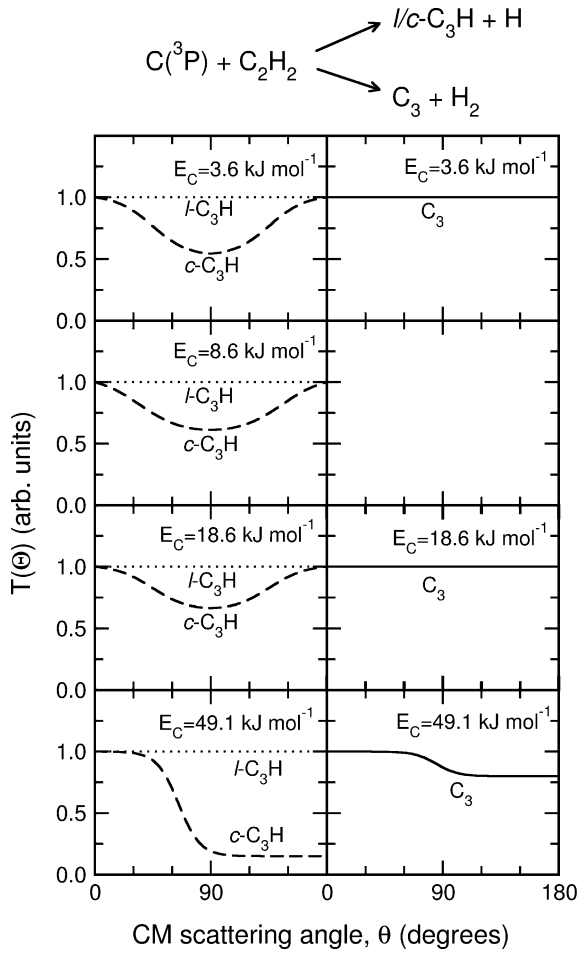

Figure 7. Best-fit CM angular distributions $T(\theta)$ for (lhs) the c-C_3H (dashed curves) and l-C_3H (dotted curves) products and (rhs) the C_3 product from the $C(^3P) + C_2H_2$ reaction at the indicated collision energies.

In the data analysis at $E_c = 49.1$ kJ mol^{-1}, we have assumed the exoergicity of channel 1b to be 11 kJ mol^{-1}, as derived in our previous work.[19] As is evident from Figure 8(lhs), the $P(E'_T)$ functions for the two different C_3H isomers are clearly different; the $P(E'_T)$ of the l-C_3H + H channel rises very fast and peaks at about 10 kJ mol^{-1}, while that of the c-C_3H + H channel has a slower rise and peaks at about 22 kJ mol^{-1}. The average product translational energy, defined as $\langle E'_T \rangle = \Sigma P(E'_T) \times E'_T/\Sigma P(E'_T)$, corresponds to a fraction of the total available energy released in translation, f_T, of 0.36 for the l-C_3H + H channel and 0.45 for the c-C_3H + H channel. As can be seen from Figure 7(lhs), at $E_c = 18.6$ kJ mol^{-1}, the $T(\theta)$ function for the linear C_3H from $C(^3P)$ is isotropic (that is, it has uniform intensity equal to 1 over all of the CM angular range (0−180°), while that for the cyclic isomer is forward peaked. These shapes provide information on the lifetimes of the linear and cyclic C_3H_2 intermediates (see section IV).

The best-fit $T(\theta)$ and $P(E'_T)$ at $E_c = 8.6$ kJ mol^{-1} for the two C_3H channels from $C(^3P)$ are depicted in Figures 7(lhs) and 8(lhs), respectively. At this E_c, both $T(\theta)$'s are backward−forward symmetric; in particular, the $T(\theta)$ of the l-C_3H isomer is isotropic, while that of c-C_3H exhibits a significant degree of polarization, as already noted at $E_c = 18.6$ and 3.6 kJ mol^{-1}.[19,33] The $P(E'_T)$ distribution of the linear isomer extends to a total energy of 10 ± 2 kJ mol^{-1}, consistent with the theoretical exoergicities of 1.5 ± 4 and 3.1 ± 4 kJ mol^{-1} calculated by Head-Gordon[1] and by Mebel,[32] respectively, while that of the cyclic isomer extends to 19.6 ± 2 kJ mol^{-1}, indicating

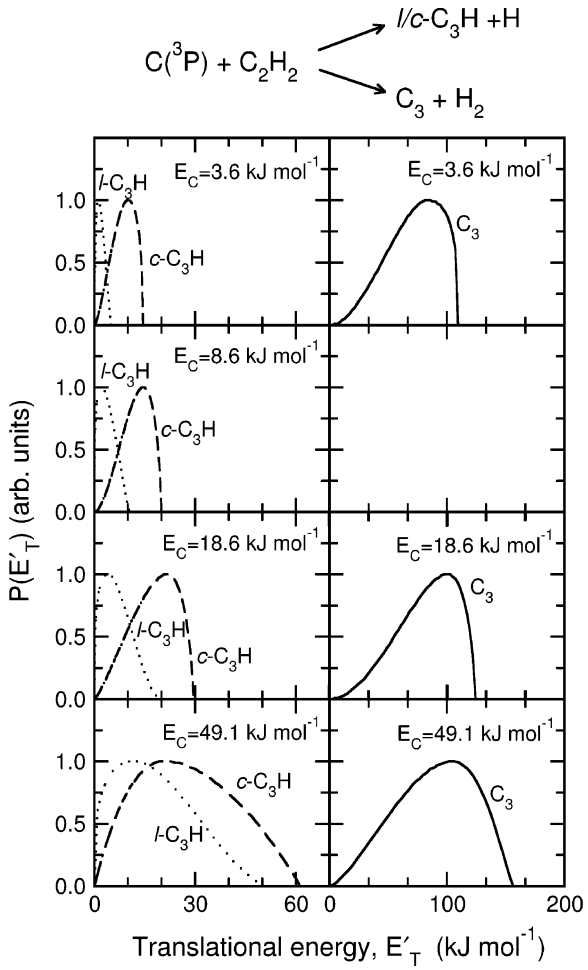

Figure 8. Best-fit CM product translational energy distributions $P(E'_T)$ for (lhs) the c-C_3H + H (dashed curves) and l-C_3H + H (dotted curves) and (rhs) the C_3 + H_2 forming channels from the $C(^3P)$ + C_2H_2 reaction at the indicated collision energies.

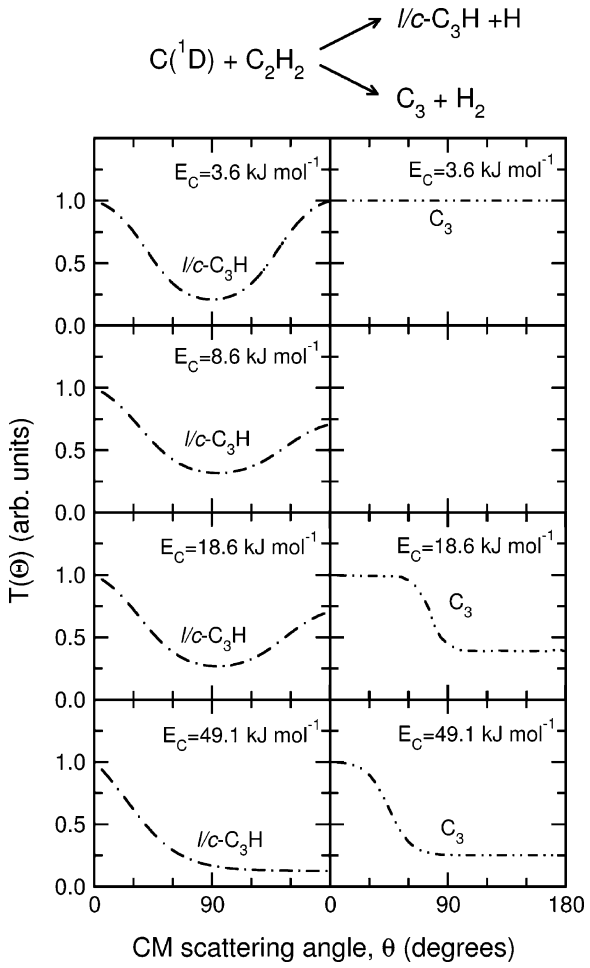

Figure 9. Best-fit CM angular distributions $T(\theta)$ for (lhs) the l/c-C_3H and (rhs) the C_3 products from the $C(^1D)$ + C_2H_2 reaction at the indicated collision energies.

that the exoergicity of channel 1b is 11.0 ± 2.0 kJ mol^{-1}, in agreement with the value derived from previous work[19] and with the theoretical values. The overall width of the angular distribution of Figure 5 is particularly sensitive to the amount of total available energy released in translation, while the shape of the LAB distribution around its maximum determines the relative ratio of linear to cyclic contributions since the linear isomer channel (1a) exhibits a very narrow LAB angular distribution because of its very small exoergicity. About 62% of the total available energy is disposed into product translation for the c-C_3H + H channel, while only 44% is disposed into products translation for the l-C_3H + H channel.

The best fits of our scattering data are most sensitive to the symmetry (or asymmetry) of the $T(\theta)$ functions and somewhat less to their degree of polarization. The best fits are also very sensitive to the rise and peaking of the $P(E'_T)$ distributions, while they are significantly less sensitive to the cutoff energy of $P(E'_T)$, especially at high E_c. As already discussed above and previously,[19] the uncertainties in the cutoff of the $P(E'_T)$ distributions at low E_c are on the order of ±2 kJ mol^{-1}, while they are higher (on the order of ±6 kJ mol^{-1}) at an E_c of 49.1 kJ mol^{-1}. With regard to the $T(\theta)$'s, the uncertainty in the $T(0°)/T(180°)$ ratio for the isotropic or backward−forward symmetric functions for both C_3H and C_3 products from the $C(^3P)$ reaction (see Figure 7) is ±0.05, while for the anisotropic $T(\theta)$'s, it is somewhat larger (about ±0.10). The uncertainty in the ratio $T(90°)/T(0°)$ for the polarized $T(\theta)$'s is on the order of ±0.20. It should be noted that the error bars in the $T(\theta)$'s are about twice as large as those for the C_3H and C_3 products from the $C(^1D)$ reaction (see Figure 9). Analogously, the uncertainty (∼±20 kJ mol^{-1}) in the cutoff energies of the $P(E'_T)$ distributions for the $C(^1D)$ reactions (see Figure 10) are significantly larger than those for the $C(^3P)$ reactions (see Figure 8).

III.3. The C_3 + H_2 Channels. In order to reproduce quantitatively the shape of the angular and TOF distributions at $m/z = 36$, two additional terms were needed in eq 3 to account for the formation of C_3 from both $C(^3P)$ and $C(^1D)$ reactions 1c and 2c

$$I_{CM}(\theta,E'_T) = w_1 \times [T(\theta)^{3P} \times P(E'_T)^{3P}]_{c-C_3H} + w_2 \times [T(\theta)^{3P} \times P(E'_T)^{3P}]_{l-C_3H} + w_3 \times [T(\theta)^{1D} \times P(E'_T)^{1D}]_{l/c-C_3H} + w_4 \times [T(\theta)^{3P} \times P(E'_T)^{3P}]_{C3} + w_5 \times [T(\theta)^{1D} \times P(E'_T)^{1D}]_{C3} \quad (4)$$

Here, the best-fit $T(\theta)$ and $P(E'_T)$ functions of the first three terms are those determined from the analysis of the $m/z = 37$ data. As already mentioned, the C_3 channel, which was explored previously at E_c = 3.6, 18.6, and 29.3 kJ mol^{-1}, has been now characterized also at E_c = 49.1 kJ mol^{-1}. The best-fit functions of the C_3 + H_2 channel from the $C(^3P)$ reaction are depicted in Figures 7(rhs) and 8(rhs).

The dotted, dashed, and dashed−dotted lines in Figures 3 and 4(rhs) are the LAB angular and TOF distributions,

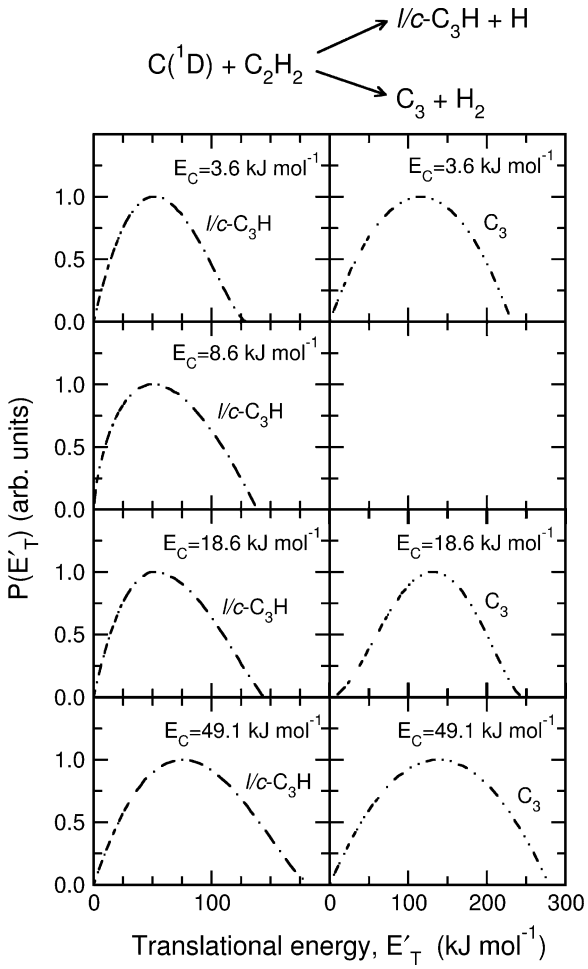

Figure 10. Best-fit CM product translational energy distributions $P(E'_T)$ for (lhs) the l/c-C_3H + H and (rhs) the $C_3 + H_2$ forming channels from the $C(^1D) + C_2H_2$ reaction at the indicated collision energies.

respectively, generated by the best-fit CM functions for the $C(^3P)$ and $C(^1D)$ reactions 1a and b and 2a and b, respectively, with $w_1 = 0.26$, $w_2 = 0.26$, and $w_3 = 0.10$ for $E_c = 49.1$ kJ mol^{-1}, while the light solid line and the dashed−double dotted line are the LAB angular and TOF distributions, respectively, generated by the best-fit CM functions for C_3 formation from the $C(^3P)$ and $C(^1D)$ reactions 1c and 2c, respectively, with $w_4 = 0.28$ and $w_5 = 0.10$.

III.4. Branching Ratios. The best-fit analysis of the data in our previous work[19] permitted the determination of the cyclic/linear C_3H ratio of cross sections $\sigma_{cyclic}/\sigma_{linear}$, which were determined to be 3.4 at $E_c = 3.5$ kJ mol^{-1} and 1.25 at $E_c = 18.5$ kJ mol^{-1}. The slight revision of these data[33] has led to the new values of 4.0 ± 0.5 and 1.2 ± 0.3, respectively. The values derived in the present study at $E_c = 8.6$ and 49.1 kJ mol^{-1} are 2.1 ± 0.3 and 1.0 ± 0.3, respectively. The trend of $\sigma_{cyclic}/\sigma_{linear}$ as a function of E_c is portrayed in Figure 11, where the predictions of the recent statistical calculations of Mebel et al.[32] are also shown.

It has also been possible to estimate the branching ratio between the competing c/l-C_3H + H and $C_3 + H_2$ reaction pathways from the $C(^3P) + C_2H_2$ reaction. Assuming, very reasonably, that the transmission through the quadrupole mass filter of the $m/z = 36$ and 37 ions are the same and that the ionization cross sections and the fragmentation patterns to C_2- and C-containing fragments of C_3H and C_3 are also the same, from the w_1, w_2, and w_4 parameters given in sections III.2 and III.3 and the relative signals at $m/z = 37$ and 36, we derive a

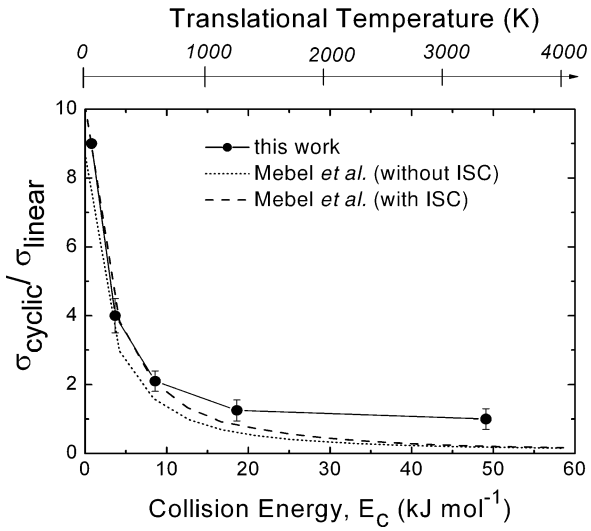

Figure 11. Ratio of cross sections for cyclic and linear C_3H formation, $\sigma_{cyclic}/\sigma_{linear}$, as a function of collision (translational) energy, E_c, as derived from crossed molecular beam studies of the $C(^3P) + C_2H_2$ reaction. The corresponding translational temperature scale is indicated on the top abscissa. The data points at $E_c = 3.6$, 8.6, 18.6, and 49.1 kJ mol^{-1} are from the present work, while that at $E_c = 0.8$ kJ mol^{-1} is from ref 19. The solid line joining the data points is drawn to guide the eye only. The ratio obtained from statistical calculations on ab initio potential surfaces by Mebel et al.[32] is reported with the dotted line (on the triplet PES only) and with the dashed line (including ISC) for comparison.

ratio of integral cross sections $\sigma(C_3 + H_2)/[\sigma(C_3 + H_2) + \sigma(C_3H + H)]$ of 0.13 ± 0.04 at $E_c = 49.1$ kJ mol^{-1}. This value can be compared with the slightly revised values of 0.50 ± 0.10 at $E_c = 3.6$ kJ mol^{-1}, 0.36 ± 0.07 at $E_c = 18.6$ kJ mol^{-1}, and 0.29 ± 0.07 at $E_c = 29.3$ kJ mol^{-1} (here, the associated uncertainties reflect the uncertainties in the relative weights obtained from the best fit-procedure). These branching ratios are depicted in Figure 12, where the recent statistical predictions[28] as well as the results of the recent pulsed CMB work of Kaiser et al.[20] at comparable E_c's are also reported.

IV. Discussion

The CM angular and translational energy distributions derived from this work and displayed in the Figures 7 and 8 contain detailed information on the dynamics of the competing reaction pathways 1a−c, while those displayed in the Figures 9 and 10 contain information on the dynamics of the corresponding reactions 2a−c. The detailed dynamics of reactions 1 and 2 will now be discussed separately in light of the triplet and singlet C_3H_2 PESs (see Figure 1).[1,21−23,26−28]

IV.1 Dynamics of c-C_3H and l-C_3H Formation from $C(^3P)$. The present DCS measurements were able to disentangle the relative contributions of the two possible C_3H isomers, which are formed from reaction 1, by analysis of their different dynamics of formation and energy release (see section III and ref 19). Before discussing the results, it is useful here to briefly recall the "osculating complex" model for chemical reactions.[29] According to this model, the ratio of the backward to forward scattering intensity in the CM, $T(\theta = 180°)/T(\theta = 0°)$, can be roughly related to the ratio between the typical rotational period of the intermediate complex, τ_{rot}, and its mean lifetime, τ, through the relation $T(\theta = 180°)/T(\theta = 0°) = \exp(-\tau_{rot}/2\tau)$. According to that relation, when the mean time for decomposition of the complex is at least five rotational periods, the $T(\theta = 180°)/T(\theta = 0°)$ ratio is nearly equal to unity, and this corresponds to a long-lived complex mechanism. When τ is

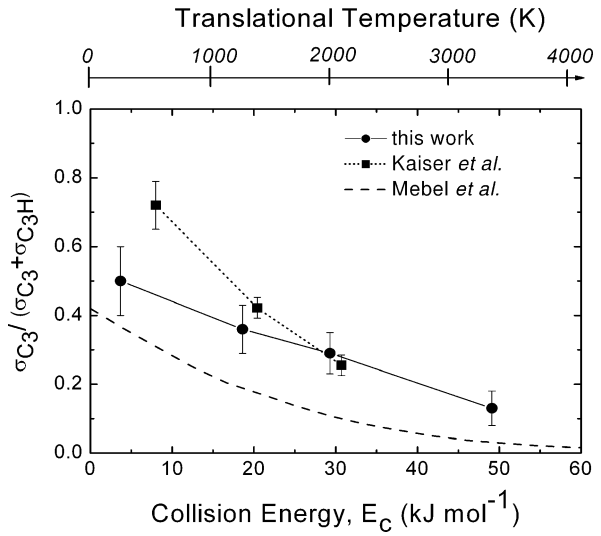

Figure 12. Branching ratio $\sigma_{C_3}/(\sigma_{C_3} + \sigma_{C_3H})$ as a function of collision (translational) energy, E_c, as derived from crossed molecular beam studies of the $C(^3P) + C_2H_2$ reaction. The corresponding translational temperature scale is indicated on the top abscissa. The solid line joining the data points (solid circles) is drawn to guide the eye only. The branching ratio obtained by Mebel et al.[32] from statistical calculations on ab initio potential surfaces including ISC is reported with a dashed line for comparison. The results of Kaiser et al.[20] obtained at three collision energies are also shown as solid squares; again, the dotted line joining the experimental points is drawn to guide the eye only.

shorter than five rotational periods, the $T(\theta = 180°)/T(\theta = 0°)$ ratio becomes significantly smaller than 1. In other words, the lifetime of the intermediate complexes can therefore be estimated from the $T(\theta)$ anisotropy. The rotational period of an intermediate complex can be estimated through the classical relation $\tau_{rot} = 2\pi I_i/L_{max}$, where I_i stands for the moment of inertia of the complex rotating around the i axis ($i = A, B, C$) and L_{max} is the maximum orbital angular momentum. For an estimation of the largest τ_{rot}, we can use the largest moment of inertia of the triplet and singlet cyclopropenylidene, propargylene, and vinylidenecarbene intermediate reaction complexes calculated by Mebel et al.[32] (see Table S1 in the supplement of material to the paper[32], as described in its ref 30). The largest moment of inertia is that around the C axis, and this is reported in Table 2 together with the estimated rotational periods for the various triplet and singlet complexes at the various experimental collision energies. L_{max} can be estimated classically by $L = \mu v_r b_{max}$, where μ and v_r are the reduced mass and relative velocity of the reactants, respectively, and b_{max} is the maximum impact parameter for reaction. The latter is estimated from the relation $\sigma = \pi b_{max}^2$, where the reaction cross section σ as a function of E_c is obtained from the rate constant[10,11] $k(T = 300\ K) = 3 \times 10^{-10}$ cm^3 molecule^{-1} s^{-1} through the approximate relation[47] $k \approx \sigma v_r$. An $E^{-1/3}$ energy dependence for σ has also been used. Table 3 reports v_r, σ, and b_{max} together with L_{max} at the various E_c's, as used for obtaining the τ_{rot} of Table 2.

As can be seen from Figure 7(lhs), the $T(\theta)$ function for the l-C_3H product (corresponding to path 1a) is isotropic at all E_c's. This indicates that the reaction channels leading to l-C_3H + H proceed through long-lived complex mechanisms, that is, intermediate C_3H_2 complexes whose lifetimes are longer than at least five rotational periods.[29] This is fully consistent with a mechanism which sees the attack of the C atom at the acetylene triple bond leading, after isomerization, to triplet propargylene (HCCCH) formation, which is the most stable C_3H_2 triplet isomer (see Figure 1) and whose lifetime is calculated[32] to range from ~5 ns at $E_c = 49$ kJ mol^{-1} up to ~2 μs at $E_c = 3.6$ kJ mol^{-1} (see Table 4). These lifetime values are orders of magnitude larger than the HCCCH rotational period (estimated to be about 1 ps at 3.6 kJ mol^{-1}, corresponding to 300 K; see Table 2). Interestingly, the $T(\theta)$ function for the c-C_3H product (corresponding to path 1b) is also backward−forward symmetric, with some degree of polarization, at the three lowest E_c's (3.6, 8.6, and 18.6 kJ mol^{-1}), while it becomes forward peaked at the highest E_c of 49.1 kJ mol^{-1} (see Figure 7(lhs)). It should be noted that in the early experiment at $E_c = 29.3$ kJ mol^{-1},[17] where the data were analyzed in terms of a single pair of $T(\theta)$ and $P(E'_T)$ functions for the two isomeric C_3H products, the overall $T(\theta)$ was somewhat forward biased, with $T(180°)/T(0°) = 0.8$. This implies, in light of the constant isotropic trend with E_c of the $T(\theta)$ for l-C_3H, that the $T(\theta)$ of c-C_3H is somewhat forward peaked at $E_c = 29.3$ kJ mol^{-1}, perfectly in line with the trend as a function of E_c outlined in Figure 8(lhs). All of this indicates that the reaction channel leading to c-C_3H + H is proceeding through a long-lived complex mechanism at least up to $E_c = 18.6$ kJ mol^{-1}, but at $E_c = 29.3$ kJ mol^{-1}, the complex lifetime becomes comparable to and then (at $E_c = 49.1$ kJ mol^{-1}) smaller than its rotational period. This interpretation is consistent with a mechanism that leads to triplet cyclopropenylidene (cyclic C_3H_2) formation, which can undergo H-atom elimination with formation of c-C_3H + H. The long-lived complex mechanism at low E_c's and the osculating complex mechanism at high E_c's are in line with the trend of the statistical calculations by Mebel et al.[32] of the triplet cyclic C_3H_2 complex lifetime (see Table 4).

The product translational energy distributions for l/c-C_3H+H formation (Figure 8(lhs)) provide information on the partitioning of the total available energy (given by collision energy + reaction exoergicity) between the translational and internal (rovibrational) energy of the products. As can be seen, the $P(E'_T)$ for the c-C_3H channel peaks far away from zero and exhibits a similar shape at all E_c's. This indicates that a rather large fraction of the total available energy is released in translation, suggesting that cyclic C_3H_2 decomposes through a rather "tight" transition state to c-C_3H+H. Conversely, the $P(E'_T)$ for the l-C_3H channel peaks very close to zero, indicating a much smaller product translational energy release and decomposition of the linear C_3H_2 intermediate via a "loose" transition state. The average fraction of energy in translation is 0.60−0.62 for c-C_3H+H at the three lowest E_c's, while it is 0.45 at $E_c = 49.1$ kJ mol^{-1}. This indicates that at high E_c, a larger fraction of the relative translational energy of the reactants is channelled into product internal excitation. The average fraction of energy in translation is nearly constant with the E_c for l-C_3H+H, being 0.39, 0.37, 0.34, and 0.35 at $E_c = 3.6$, 8.6, 18.6, and 49.1 kJ mol^{-1}, respectively. Therefore, the l-C_3H product is internally more excited ($f_{int} \approx 0.60-0.65$) than the c-$C_3H$ product ($f_{int} \approx 0.40-0.55$).

Our findings that the $P(E'_T)$ for the c-C_3H + H channel reflects a somewhat tight exit transition state,[29] while that for the l-C_3H+H channel reflects a loose exit transition state,[29] are corroborated by the theoretical work of Mebel et al.[32] These authors, indeed, found that H loss takes place via loose variational transition states, with the ones to form l-C_3H significantly looser (they have lower vibrational frequencies) than those leading to the tighter c-C_3H isomer product.

An important point to note is that both c-C_3H and l-C_3H observed experimentally and originating from the $C(^3P)$ reaction can also be formed from the singlet intermediates (cyclopropenylidene and propargylene/vinylidenecarbene, respectively) once they have been reached by ISC from the triplet PES. In

TABLE 2: Rotational Periods of Various Triplet and Singlet Intermediate Complexes; the Moments of Inertia of the Same Complexes for Rotation around the *C* axis Are Also Reported

complex	triplet c-C_3H_2	triplet l-C_3H_2	triplet H_2CCC	singlet c-C_3H_2	singlet l-C_3H_2	singlet H_2CCC
E_c (kJ mol^{-1})			rotational periods (ps)			
3.6	0.82	1.25	1.25	0.76	1.25	1.25
8.6	0.60	0.95	0.95	0.58	0.94	0.95
18.6	0.46	0.73	0.73	0.45	0.72	0.73
49.1	0.33	0.53	0.53	0.33	0.53	0.53
			moment of inertia (kg m^2)			
I_C	5.2×10^{-46}	8.2×10^{-46}	8.2×10^{-46}	5.0×10^{-46}	8.1×10^{-46}	8.2×10^{-46}

TABLE 3: Relative Velocity v_r, Reactive Cross Section σ, Maximum Impact Parameter b_{max}, and Maximum Orbital Angular Momentum L_{max} at Various Collision Energies E_c

E_c (kJ mol^{-1})	v_r (m s^{-1})	σ (Å^2)	b_{max} (Å)	L_{max} (kg m^2 s^{-1})
3.6	955	31.4	3.16	4.11×10^{-33}
8.6	1447	23.6	2.75	5.43×10^{-33}
18.6	2129	18.3	2.42	7.03×10^{-33}
49.1	3458	13.3	2.06	9.71×10^{-33}

fact, ISC from triplet to singlet PESs is known to occur because it is the only path leading to the spin-forbidden $C_3 + H_2$ channel (see below). Once the singlet cyclopropenylidene (C_3H_2) is formed, it can undergo CH bond cleavage with the formation of c-C_3H + H as well as isomerization to singlet propargylene (HCCCH) and/or singlet vinylidenecarbene (H_2CCC), both of which can, in turn, lead to l-C_3H formation by CH bond rupture.

It should also be noted that c/l-C_3H formation from the singlet C_3H_2 intermediates is expected to proceed via a long-lived complex mechanism, considering that the lifetimes of the singlet complexes (reached by ISC) are calculated to be very long with respect to H elimination from about 195 (64) ps at $E_c = 49.1$ kJ mol^{-1} up to 64 (1.8) ns at $E_c = 3.6$ kJ mol^{-1} for linear (cyclic) singlet C_3H_2 (see Table 4).[32]

IV.2. Cyclic C_3H/Linear C_3H Ratios. As shown in Figure 11, the ratio $\sigma_{cyclic}/\sigma_{linear}$ is found to decrease with increasing E_c, from ~9 at $E_c = 0.8$ kJ mol^{-1} to 1.0 ± 0.3 at $E_c = 49.1$ kJ mol^{-1} (the value at $E_c = 0.8$ kJ mol^{-1} in Figure 11 is from ref 19). These results contradict those obtained from dynamical calculations on the triplet PES, both those from quantum scattering studies in reduced dimensionality by Buonomo and Clary,[24] which predicted l-C_3H to be preferentially formed at any E_c sampled between $E_c = 5$ ($\sigma_{cyclic}/\sigma_{linear} < 0.02$) and 70 kJ mol^{-1} ($\sigma_{cyclic}/\sigma_{linear} \sim 0.17$), and those by Takayanagi[25] who oppositely predicted overwhelmingly dominant c-C_3H production between $E_c = 0.1$ ($\sigma_{cyclic}/\sigma_{linear} > 10^2$) and 58 kJ mol^{-1} ($\sigma_{cyclic}/\sigma_{linear} \sim 10^4$). The experimental ratio is also at strong variance with the results of QCT calculations on a full-dimensional ab initio triplet PES by Bowman and co-workers,[26] who found l-C_3H to be preferentially formed at all E_c's investigated, from 5 ($\sigma_{cyclic}/\sigma_{linear} \sim 0.07$) to 40 kJ mol^{-1} ($\sigma_{cyclic}/\sigma_{linear} \sim 0.05$). The theoretical $\sigma_{cyclic}/\sigma_{linear}$ ratios calculated by Buonomo and Clary and by Bowman and co-workers are not shown in Figure 11 because, being too small, they would not be distinguishable on the scale of the figure. For the opposite reason, the results of Takayanagi are also not plotted because they are much too large for the scale of the figure.

In contrast to the sharp disagreement noted with the results of dynamical calculations on the triplet C_3H_2 PES, good qualitative and semiquantitative agreement is found between the present experimental results and those of the statistical calculations by Mebel et al.[32] These authors have applied RRKM theory for isomerization and dissociation steps within the same multiplicity and radiationless transition- and nonadiabatic transition-state theories for singlet−triplet ISC rates. On the triplet PES, the calculated $\sigma_{cyclic}/\sigma_{linear}$ as a function of E_c decreases from 8.7 at 0 kJ mol^{-1} to approximately 0.2 at 50 kJ mol^{-1} (see dotted line in Figure 11), while by including ISC with triplet−singlet transition rate constants calculated by employing nonadiabatic transition-state theory, the ratio decreases from ~10 at 0 kJ mol^{-1} to ~0.2 at 50 kJ mol^{-1} (see dashed line in Figure 11). According to Mebel's work, both *trans*-C_3H_2 (propenylidene) and cyclic C_3H_2 can be formed in the initial reaction step (see Figure 1); because the isomerization processes for the C_3H_2 species occur much faster than their dissociation, an equilibrium concentration of the various C_3H_2 isomers is reached before they decompose, and this is at the basis of the statistical calculations. The trends in branching ratios have been rationalized by Mebel et al.[32] by considering the energies and tightness of transition states involved in the dissociation processes. The rate constant for H elimination from linear C_3H_2 to form l-C_3H + H is calculated to increase 100 times faster, when E_c increases from 0 to 60 kJ mol^{-1}, than that for the H loss from cyclic C_3H_2 to produce c-C_3H + H.[32] Therefore, on statistical grounds, it is not surprising that the most exoergic channel leading to c-C_3H is preferentially formed at low E_c, while the relative importance of the less exoergic l-C_3H channel increases considerably with increasing E_c. As can be seen in Figure 11, the statistical predictions without ISC are in reasonably good agreement, and those including ISC are in very good agreement with experiment at low E_c's; however, both predictions appear to increasingly underestimate the formation of c-C_3H with increasing E_c. This could be ascribed to some dynamical effects in the dissociation of the cyclic and linear C_3H_2 isomers, which could become important at high E_c's.

As discussed above, the c-C_3H and l-C_3H isomers formed from the $C(^3P) + C_2H_2$ reaction can originate from the decomposition of both triplet and singlet intermediates after ISC. The experiment cannot tell us quantitatively which fraction of c-C_3H comes from triplet cyclic C_3H_2 and which one comes from singlet cyclic C_3H_2. However, from the experimental observation of the $C_3 + H_2$ channel, we know that ISC occurs with high probability, and therefore, it is reasonable to expect that a significant fraction of c/l-C_3H also originates from the singlet intermediates. According to the statistical calculations including ISC by Mebel et al.[32] at $E_c = 4.2$ kJ mol^{-1} (at which a $\sigma_{cyclic}/\sigma_{linear}$ ratio of 3.85 is predicted, in good agreement with the ratio of 4.0 ± 0.5 derived from the experiment at $E_c = 3.6$ kJ mol^{-1}), 12.2% of the predicted 50.8% of c-C_3H originates from triplet cyclic C_3H_2, while 38.6% is from singlet cyclic C_3H_2. Of the predicted 13.2% of l-C_3H, 3.6% originates from triplet HCCCH and 0.5% from triplet H_2CCC, while 3.5% originates from singlet H_2CCC and 5.6% from singlet HCCCH. The calculated remaining 36.0% of the reaction products is represented by the $C_3 + H_2$ channel, which occurs via ISC (24.4% is computed to originate from singlet H_2CCC, with 11.6% produced from singlet HCCCH). Similar estimates at the different collision energies (from 0 to 62.8 kJ mol^{-1}) are

TABLE 4: Statistical Lifetimes of Triplet and Singlet Complexes as a Function of E_c (Interpolated from the Theoretical Results in Table 2 of Ref 30) for the $C(^3P) + C_2H_2$ Reaction

complex	triplet c-C_3H_2 → c-C_3H+ H	triplet l-C_3H_2 → l-C_3H+ H	singlet c-C_3H_2 → c-C_3H+ H	singlet l-C_3H_2 → l-C_3H+ H	singlet l-C_3H_2 → $C_3 + H_2$	singlet H_2CCC → $C_3 + H_2$
E_c (kJ mol^{-1})						
3.6	260 ps	2060 ns	1790 ps	57 ns	26 ns	6 ns
8.6	157 ps	611 ns	1008 ps	17 ns	18 ns	4 ns
18.6	67 ps	101 ns	440 ps	3 ns	6.5 ns	1.8 ns
49.1	12 ps	5 ns	64 ps	195 ps	2 ns	292 ps

reported in Table S2 of the supporting information of Mebel et al.[32] It is interesting to note, in light of these statistical calculations, that the ratio $\sigma_{cyclic}/\sigma_{linear}$ coming exclusively from the triplet surface is predicted to be 3.0, while that from the singlet surface is 4.24. That is, at low E_c, both triplet and singlet intermediates undergo H loss to form c-C_3H + H preferentially rather than l-C_3H + H. This statistical result on the triplet PES of Mebel et al.[32] is very different from the above dynamical results on the PES of the same multiplicity. Obviously, it is desirable to have dynamical calculations on a more accurate triplet PES and also with inclusion of ISC.

IV.3. Dynamics of C_3 Formation from $C(^3P)$. The $T(\theta)$ function for C_3 formation from the $C(^3P)$ reaction is isotropic at the three lowest E_c's and becomes slightly forward biased at $E_c = 49.1$ kJ mol^{-1} (see Figure 8(rhs)). It should be noted that C_3 formation was found to have a nearly isotropic $T(\theta)$ also at $E_c = 29.3$ kJ mol^{-1},[17] with only a slight preference for forward scattering, in line with the present results. This trend of $T(\theta)$ with E_c indicates that the $C_3 + H_2$ pathway is proceeding through C_3H_2 complex(es), whose lifetimes are significantly longer than their rotational periods. From the extent of the translational energy release at the various E_c's (see Figure 8(rhs)), the exoergicity of the $C_3 + H_2$ forming channel is estimated to be $\sim 105 \pm 10$ kJ mol^{-1}, in agreement with the literature data on the relevant heats of formation ($\Delta_f H°_0(C(^3P)) = 709.5 \pm 2$ kJ mol^{-1},[48] $\Delta_f H°_0(C_2H_2) = 227.3 \pm 0.8$ kJ mol^{-1},[48] and $\Delta_f H°_0(C_3) = 831 \pm 13$ kJ mol^{-1} [49]), which gives $\Delta_r H°_0 = -106 \pm 16$ kJ mol^{-1}. It should be noted that the theoretical exoergicity of channel 1c calculated by Mebel et al.[32] is 127.8 kJ mol^{-1} (with an estimated uncertainty of at least $\pm$ 10 kJ mol^{-1}),[50] somewhat larger than that estimated from the literature heats of formation and experiment. Clearly, there is a need for a more precise determination of the heat of formation of C_3. In any case, from the extent of the $P(E'_T)$, it is inferred that C_3 is formed in its ground-state linear form $X^1\Sigma_g^+$ (channel 1c). This can only be rationalized by invoking ISC between the triplet and singlet PES leading to a singlet C_3H_2 intermediate which, by H_2 elimination, can produce $C_3(X^1\Sigma_g^+)$. Mebel et al.[23] indeed suggested in their earlier work that formation of linear C_3 involves ISC from triplet propargylene to singlet cyclopropenylidene (the most stable C_3H_2 isomer; see Figure 1), which then isomerizes to singlet H_2CCC, which undergoes a three-center H_2 elimination. However, in the most recent work, Mebel et al.[32] were able to locate another singlet−triplet seam of ISC which is significantly lower in energy and resides in close vicinity to singlet linear C_3H_2 (propargylene; see Figure 1). Therefore, ISC from triplet to singlet propargylene is expected to be the main nonadiabatic pathway in the $C(^3P) + C_2H_2$ reaction.[32] Again, isomerization reactions between the three singlet C_3H_2 isomers are calculated to be much faster than their dissociation.[32] Molecular hydrogen elimination can take place from both H_2CCC (via a three-center elimination process) and HCCCH (via a four-center process), with the rate for the former being statistically about twice that for the latter at low E_c ($\sim$4 kJ mol^{-1}) and about three times larger at high E_c ($\sim$50 kJ mol^{-1}) (see Table S2 in the supporting information of Mebel et al.[32]). The experimentally determined average fraction of total available energy released in product translation is 0.66 at $E_c = 3.6$ and 18.6 kJ mol^{-1},[19] and it decreases to 0.57 at $E_c = 49.1$ kJ mol^{-1}, a value very similar to that (0.564) already found[17] at $E_c = 29.3$ kJ mol^{-1}. These large values are an indication that a high potential barrier is present in the exit channel of this reaction pathway; indeed, an exit barrier of 98 kJ mol^{-1} (with respect to the products) has been calculated for H_2 elimination from singlet H_2CCC and a slightly lower one (94 kJ mol^{-1}) for H_2 elimination from singlet HCCCH (see Figure 1).[32] The fact that the fraction of energy in translation decreases somewhat with increasing E_c indicates that the extra translational energy of the reagents is mainly channelled into internal excitation of the products.

The backward−forward symmetric $T(\theta)$'s for the C_3 product determined in this work (Figure 8(rhs)) are fully consistent with Mebel's picture in which the lifetime of triplet propargylene is calculated to range from about 2 μs at $E_c = 3.6$ kJ mol^{-1} to 5 ns at $E_c = 49.1$ kJ mol^{-1} (see Table 4), that is, the statistical calculations of the C_3H_2 intermediate undergoing ISC predict a long-lived complex mechanism even at an E_c on the order of 50 kJ mol^{-1}. ISC from triplet propargylene competes with H elimination to form l-C_3H. Although at $E_c = 0$ kJ mol^{-1}, the ISC rate constant is about 3 orders of magnitude higher than that for H elimination;[32] at low E_c, a long-lived complex mechanism fully applies for H_2 elimination, at least at low and moderate E_c's. While the rate of ISC remains essentially constant (rises very slowly) with E_c, the rate of H elimination is calculated[32] to increase by 3 orders of magnitude as E_c is increased from 0 to 50 kJ mol^{-1}.

IV.4. Comparison with previous pulsed CMB work. Comparison of the present results with those of early[1,12−14] and recent[20] CMB investigations using pulsed beams is in order. Previous CMB experiments at $E_c = 8.8$, 28.0, and 45.0 kJ mol^{-1} by Kaiser et al.,[12,13] which were very recently confirmed by a new series of experiments,[20] indicated a preferential pronounced forward scattering of the C_3H product at low E_c and a symmetric scattering at high E_c, a trend which is opposite to the present results and is also contradicted by the Doppler shift measurements at very low E_c in pulsed CMB experiments with H-atom detection.[19] Kaiser et al. suggested that at low E_c, c-C_3H is formed through a short-lived triplet cyclopropenylidine (cyclic C_3H_2) intermediate in a direct fashion, leading to a forward-peaked $T(\theta)$, whereas l-C_3H is formed via a triplet propargylene (HCCCH) intermediate and is characterized by a backward−forward symmetric angular distribution. As E_c increased, the $m/z = 37$ CM angular distribution culminated in an isotropic $T(\theta)$ at $E_c = 45.0$ kJ mol^{-1} leading solely to the l-C_3H isomer. Notably, at that time,[12,13] the authors ruled out the interpretation that a long-lived HCCCH (propargylene) collision complex could contribute to an isotropic $T(\theta)$ for the l-C_3H isomer because it was argued, by comparison with the related reaction $C(^3P) + CH_3CCH$, that the lifetime of triplet propargylene is expected to be smaller than the rotational period of the HCCCH

reaction intermediate. It was instead argued that the l-C_3H-forming channel exhibiting an isotropic $T(\theta)$ originated in the rotation of a symmetric reaction intermediate (HCCCH) around the C_2 symmetry axis, fragmenting to l-C_3H + H (that is, the two H atoms can be interconverted through a rotation). In this regard, the notion that the propargylene intermediate is not long-lived at thermal energies was challenged by subsequent ab initio and RRKM calculations by Guadagnini et al.,[22] who calculated unimolecular lifetimes for intermediate propargylene complexes from the $C(^3P) + C_2H_2$ reaction to be 2500 and 1900 ps at 300 and 1000 K, respectively, with an upper limit for the rotational period of the complex being ≈44 ps (that is, on the order of 50 times shorter that the complex lifetime). In contrast to the l-C_3H product, the estimated forward scattering of the c-C_3H product was rationalized[12−14] by invoking an impact-parameter-dependent mechanism within the framework of simple capture theory, whereby increasing the collision energy translates into a reduction of the maximum impact parameter leading to reaction. As such, it was speculated that as E_c rises, reactive trajectories with large impact parameters, which can account for the forward peaking, are quenched. The interpretation of the experimental results was assisted by combined coupled-cluster ab initio electronic structure calculations of the triplet intermediates, product structures, and energetics.[1] The reaction mechanisms derived by Kaiser et al.[12−14] are quite surprising because addition−elimination reactions of this type leading to two very weakly exoergic product channels and proceeding through very strongly bound reaction intermediates, such as triplet cyclopropenylidene/propargylene/vinylidenecarbene (see Figure 1), are usually expected to proceed via a long-lived complex mechanism at low E_c and eventually through an "osculating complex" mechanism at high E_c.[29,47]

In order to show the sensitivity of our experimental data to the anisotropy of the CM angular distribution (that is, the $T(\theta)$ function), in Figure 13, we compare our experimental LAB angular distributions (dots) measured at $E_c = 3.6$, 8.6, and 18.6 kJ mol^{-1} with the predictions (lines) of the CM functions $T(\theta)$ and $P(E'_T)$ derived by Kaiser et al.[20] from the analysis of their most recent experimental data. The same $E^{-1/3}$ energy dependence of the integral cross section as that in ref 20 was used in the simulations. Specifically, the CM functions at $E_c = 8.0$ and 20.4 kJ mol^{-1} from ref 20 are used to simulate our experimental data at $E_c = 8.6$ and 18.6 kJ mol^{-1}, respectively. The same CM functions derived for $E_c = 8.0$ kJ mol^{-1} in ref 20 are also used to simulate our experimental angular distribution at $E_c =$ 3.6 kJ mol^{-1}; this is a conservative assumption because, on the basis of the trend reported in Figure 5 of ref 20 (which is similar to the trend reported in Figure 8 of ref 12), the $T(\theta)$ function at $E_c = 3.6$ kJ mol^{-1} would actually be expected to be even more forward peaked than that at 8.0 kJ mol^{-1}. In these simulations, the $C(^1D)$ contribution is kept identical to that derived in our best-fit simulations. As can be seen from Figure 13 at the lowest E_c, the total LAB angular distribution predicted by Kaiser's functions is strongly shifted in the forward direction (small angles) with respect to the experiment and therefore is at the intermediate E_c, with the shifting being smaller at the higher E_c of 8.6 kJ mol^{-1}. These clear deviations are the consequence of the increasingly forward peaking of the $T(\theta)$ function with decreasing E_c derived in the work of Kaiser et al.[12,13,20] Our data and best-fit analysis show clearly that the $T(\theta)$ for both c-C_3H and l-C_3H formation is perfectly backward−forward symmetric at all of these three collision energies and, in marked contrast to the results of Kaiser et al., does not become increasingly more forward peaked as E_c decreases. As already

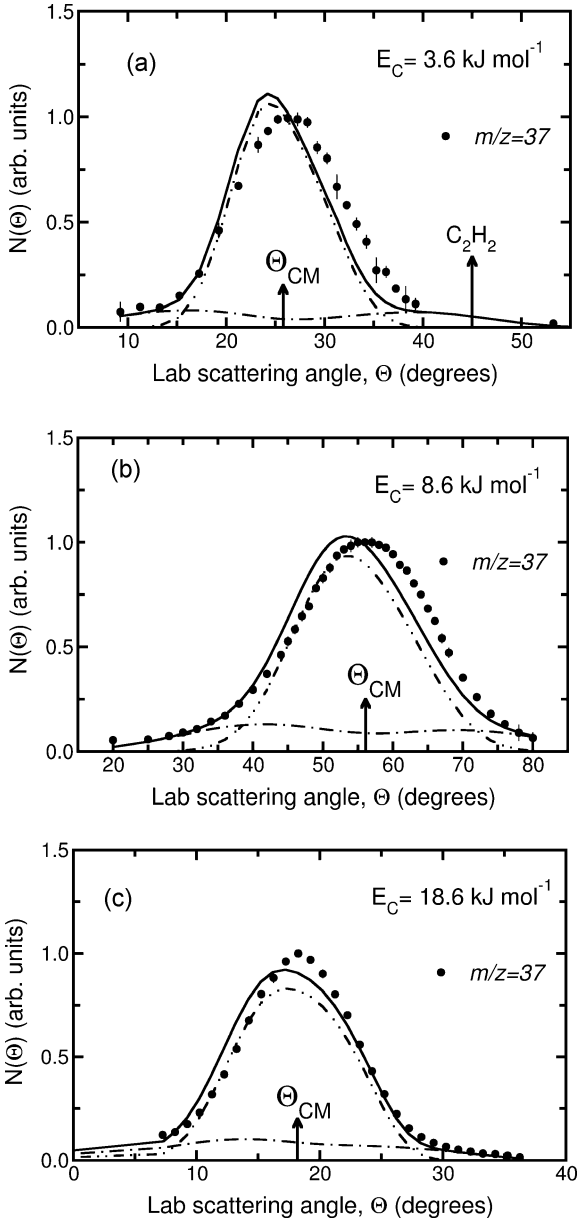

Figure 13. Laboratory angular distribution, $N(\Theta)$ of C_3H products at $m/z = 37$ (solid circles) from the reactions $C(^3P,^1D) + C_2H_2$ at three indicated E_c's from our previous[19] and present work compared with simulations using CM product angular and translational energy distributions from the work of Kaiser et al.[12,20] for the $C(^3P)$ reaction and our best-fit functions for the $C(^1D)$ reaction (see text for details).

discussed, the long-lived complex mechanism invoked to rationalize the reaction dynamics observed in our study is fully corroborated by the statistical calculations of Mebel et al.[32] on the lifetimes of the various reaction intermediates as a function of E_c (see also Table 4).

It is also worth comparing the present results for the $C_3 + H_2$ channel with those recently obtained by Kaiser and co-workers.[20] Also for this channel, there is a considerable disagreement between our results and those obtained by Kaiser and co-workers. In fact, in their study, the $T(\theta)$ of the C_3 channel is already considerably forward peaked ($T(180°)/T(0°) \approx 0.55$) at the quite low E_c of 8.0 kJ mol^{-1} and becomes strongly forward peaked at $E_c \approx 30$ kJ mol^{-1} (see Figure 5 in ref 20). This indicates that the lifetime of the triplet reaction complex leading to ISC and of the singlet intermediate that then leads to H_2 elimination is already somewhat smaller than its rotational period at 8 kJ mol^{-1} and much smaller than that at 31 kJ mol^{-1}

(at which $T(180°)/T(0°) \approx 0.15$). Actually, Kaiser and co-workers[20] used their derived anisotropy of the $T(\theta)$ function for the C_3 channel to estimate the lifetime of the singlet vinylidenecarbene intermediate (H_2CCC) leading to $C_3 + H_2$. According to their estimates, the H_2CCC lifetime decreases from 0.57 to 0.12 ps when E_c increases from 8 to 31 kJ mol^{-1}. This is a rather surprising result considering that ISC from a very long lived triplet intermediate is invoked also by them[20] to rationalize the formation of $C_3 + H_2$ from $C(^3P) + C_2H_2$. Those lifetime values are in strong contrast with Mebel's statistical calculations[32] of the triplet and singlet complex lifetimes (see Table 4). The results of Kaiser and co-workers[20] are at odds with our findings in which the $T(\theta)$ for C_3 formation is actually isotropic up to $E_c = 18.6$ kJ mol^{-1} and becomes slightly forward peaked only at 49.1 kJ mol^{-1} (see Figure 7(rhs)).

IV.5. $C_3/(C_3 + C_3H)$ Branching Ratio. As already discussed, formation of $C_3 + H_2$ from $C(^3P) + C_2H_2$ requires a nonadiabatic transition to take place between the triplet and the singlet PESs. The branching ratio of cross sections $\sigma_{C_3}/(\sigma_{C_3}+\sigma_{C_3H})$ of 0.50 ± 0.10 derived from the present study at the lowest E_c of 3.6 kJ mol^{-1} (see Figure 12) indicates that ISC is facile in this system. Interestingly, Takahashi et al.[21] postulated a mechanism for the $C(^3P) + C_2H_2$ reaction that includes ISC and the formation of a singlet intermediate. Mebel et al.[32] have shown that the nonadiabatic transition of triplet to singlet propargylene occurs via the triplet−singlet seam of crossing labeled as intersystem crossing in Figure 1. As pointed out by Guadagnini et al.[22] and confirmed by Mebel et al.,[32] the triplet C_3H_2 adduct is very long lived even at high temperatures (collision energies). As a result, the system may have time enough to undergo ISC from triplet to singlet propargylene, which then can readily lead to $C_3 + H_2$ directly or via isomerization to H_2CCC.

The branching ratio $\sigma(C_3)/(\sigma(C_3) + \sigma(C_3H))$ was found to increase with decreasing E_c (see Figure 12) (analogously to the σ(c-C_3H)/σ(l-C_3H) ratio (see Figure 11)), as one may reasonably expect from the trend with E_c of the lifetimes of the intermediate C_3H_2 complex(es); in fact, the complex lifetimes increase with decreasing E_c, as does the probability of ISC (see Table 4).[32] These results confirm the original finding at $E_c = 29.3$ kJ mol^{-1} that intersystem crossing is facile and important in the $C(^3P) + C_2H_2$ reaction.[16−18]

Our experimental values at four E_c's covering the range from 3.6 to 49.1 kJ mol^{-1} can be compared with the theoretical predictions by Mebel et al.,[32] which are reported as a dashed line in Figure 12. Mebel et al. used radiationless transition- and nonadiabatic transition-state theories (TST) for singlet−triplet ISC rates. The results shown in Figure 12 are those obtained using nonadiabatic TST, which are very close to those obtained by radiationless transition theories. The lifetime of triplet propargylene becomes shorter as E_c increases (see Table 4), making ISC to the singlet PES less probable as E_c increases; at low E_c the branching ratio of C_3 is particularly sensitive to the rate of ISC. As can be seen in Figure 12, the comparison between experiment and statistical theory is rather satisfying, although theory appears to underestimate the experimental results, indicating that the intersystem crossing is somewhat underestimated theoretically.

The experimental value of 0.50 ± 0.10 at $E_c = 3.6$ kJ mol^{-1} is found to be in agreement (see Figure 12) with the result of the kinetic study of the $C(^3P) + C_2H_2$ reaction at 300 K (corresponding to $E_c \approx 3.6$ kJ mol^{-1}), giving an upper limit for the branching ratio for H formation of 0.53 ± 0.04.[30]

Plotted in Figure 12 are also the results of the recent determination by Kaiser and co-workers.[20] As can be seen, the branching ratio derived by Kaiser et al. as a function of E_c exhibits an increase with decreasing E_c which is steeper than ours. In particular, their value of 0.73 ± 0.07 derived at $E_c = 8.0$ kJ mol^{-1} is larger (by nearly 50%) than our estimated value at the lower E_c of 3.6 kJ mol^{-1}; it is also larger than the kinetic value of 0.47 ± 0.04 derived at 300 K.[30]

IV.6. Dynamics of c/l-C_3H and C_3 formation from $C(^1D)$. As can be seen from Figure 10(lhs), the $T(\theta)$ function for the l/c-C_3H (corresponding to paths 2a and 2b) is backward−forward symmetric at the lowest E_c of 3.6 kJ mol^{-1}, becomes slightly forward biased as E_c increases to 8.6 and 18.6 kJ mol^{-1}, and is strongly forward peaked at the highest E_c of 49.1 kJ mol^{-1}. This indicates that the reaction channel leading to H elimination proceeds through a long-lived complex mechanism at the lowest E_c and through an intermediate complex which begins to osculate as E_c is raised to approximately 20 kJ mol^{-1}.

Mebel et al.[32] have calculated rate constants as a function of the available internal energy of each triplet and singlet intermediate or transition state, where the internal energy was taken as a sum of the energy of chemical activation in the $C(^3P) + C_2H_2$ reaction and the collision energy, assuming that a dominant part of the latter is converted to internal vibrational energy. With respect to the $C(^3P)$ reaction, the energy of the chemical activation of the $C(^1D) + C_2H_2$ reaction is about 122 kJ mol^{-1} larger (corresponding to the excitation energy of $C(^1D)$). On the basis of the trends of the intermediate lifetimes with E_c reported by Mebel et al.,[32] we expect that the lifetimes of singlet c-C_3H_2, HCCCH, and H_2CCC for the $C(^1D)$ reaction are much shorter than the values reported for the $C(^3P)$ reaction (see Table 4). Very recently, Mebel[50] has also calculated the RRKM rate constants for all reaction steps on the singlet PES of the $C(^1D) + C_2H_2$ reaction at various collision energies. He finds that the lifetime of singlet cyclic C_3H_2 for H elimination decreases from a few picoseconds at $E_c = \sim 4$ kJ mol^{-1} to about 1 picoseconds at $E_c = \sim 50$ kJ mol^{-1}, that is, as E_c increases, the lifetime of singlet cyclic C_3H_2 for the $C(^1D)$ reaction ranges from about 500 to 40 times shorter than that for the $C(^3P)$ reaction (see Table 4). These lifetime values for the $C(^1D)$ reaction are qualitatively and quantitatively consistent with the experimental trends that suggest a long-lived complex mechanism at low E_c and an osculating one as E_c is raised. Similar orders of magnitude of difference with respect to the $C(^3P)$ reaction were also found by Mebel[50] for the lifetimes of the other singlet isomers with respect to H and H_2 elimination. For instance, the lifetime of singlet H_2CCC (which is statistically calculated to be the main intermediate leading to H_2 elimination) with respect to $C_3 + H_2$ formation ranges from about 20 ps at the lowest E_c to about 7 ps at the highest E_c (compare with the corresponding values in Table 4 for the $C(^3P)$ reaction, which are 6 ns and 292 ps, respectively).[50]

The $T(\theta)$ for C_3 formation is also backward−forward symmetric at low E_c, while it is significantly forward peaked at 18.6 kJ mol^{-1} and even more so at 49.1 kJ mol^{-1} (Figure 9(rhs)) This reflects the fact that the reaction proceeds through a long-lived complex mechanism at low E_c and an osculating complex mechanism at higher E_c. This finding correlates with the trend of the statistical lifetimes of the relevant (HCCCH and H_2CCC) singlet intermediates leading to $C_3 + H_2$, as calculated by Mebel.[50] Again, although the information about the CM functions of the $C(^1D)$ reaction are considerably less accurate than that for the $C(^3P)$ reaction, we note that there is a satisfactory agreement between the statistical predictions and experiment. One should also note that the $C(^1D)$ reaction may not be fully statistical; in fact, the CM angular distributions at

relatively high E_c indicate that we are in the osculating regime, which probably means that full equilibration of energy among all vibrational modes does not happen. Consequently, although the calculated rates are still within the applicability limit of RRKM theory, RRKM may not be quite accurate.[50] Dynamical calculations on the $C(^1D)$ reaction would be very valuable here.

Regarding the product translational energy release, the $P(E'_T)$ for the $C_3H + H$ channels peaks away from zero (Figure 10-(lhs)) and reflects an average fraction of total available energy in translation of about 0.44, nearly constant with E_c. This fraction is larger than that found for l-$C_3H + H$ (0.35−0.39) from $C(^3P)$, while it is smaller than that for c-$C_3H + H$ (0.60−0.45); however, it appears to be close to the average values (between c- and l-C_3H) of the $C(^3P)$ reaction. The $P(E'_T)$ for the H_2 channel (Figure 10(rhs)) reflects about 50% of energy in translation, independent of E_c. This fraction is larger than that for the H channel because of the presence of a high exit barrier for H_2 elimination. Interestingly, the fractional value of 0.50 is lower than that for the $C_3 + H_2$ channel from the $C(^3P)$ reaction via ISC, where values of 0.66−0.57 were found; this implies that the molecular products are internally significantly more excited in the $C(^1D)$ reaction, indicating that part of the electronic energy is channelled into product internal excitation.

The results are consistent with a mechanism that sees $C(^1D)$ attacking the triple bond of acetylene to form singlet c-C_3H_2 (the most stable of all C_3H_2 isomers; see Figure 1), which can undergo CH bond cleavage forming c-$C_3H + H$ or isomerize to singlet HCCCH and H_2CCC, which in turn can produce l-$C_3H + H$ by H loss and $C_3 + H_2$ by H_2 elimination.

One remaining question is whether ISC from singlet to triplet PES is important. According to Mebel's unpublished results,[50] the ISC rate for the $C(^1D)$ reaction is too slow (and practically independent of the collision energy) to compete with isomerization and dissociation.

It is worthwhile to compare the present results on the $C(^1D) + C_2H_2$ reaction dynamics with the results of the previous study reported by Kaiser et al.,[27] who combined CMB experiments with electronic structure calculations of the singlet C_3H_2 PES. TOF spectra were recorded at $m/z = 37$ at $E_c = 45$ and 109 kJ mol^{-1}. These were found to be identical to those recorded at $m/z = 36$, and this led to the conclusion that the reaction leads only to the H-elimination channel at these E_c's. In the pulsed beam work, the presence of large concentration of C_3 in the C beam together with the unfavorable kinematics (low TOF resolution because of the high CM velocity) may have represented a complication that prevented the detection of C_3 products. It was concluded that the reaction proceeds via direct stripping dynamics on the singlet surface via addition of the C atom to the π-orbital of acetylene to form a highly rovibrationally excited, short-lived cyclic C_3H_2 intermediate which decomposes by H emission to form solely c-$C_3H + H$. The $T(\theta)$ function was found to be strongly forward peaked at $E_c = 45$ kJ mol^{-1}, all confined between 0 and 90°, and even more strongly peaked at $E_c = 109$ kJ mol^{-1}, all confined between 0 and 50°. Our $T(\theta)$ at $E_c = 49.1$ kJ mol^{-1} exhibits also a pronounced forward peaking, but with some intensity also in the backward hemisphere (see Figure 9(rhs)). The fraction (0.50) of energy in product translation found in our study is in agreement with that (0.50−0.55) determined by Kaiser et al. at $E_c = 45$ kJ mol^{-1}. However, in the pulsed CMB study, no evidence of $C_3 + H_2$ formation was found. This is quite surprising because the $C_3 + H_2$ pathway, which is spin-allowed for $C(^1D)$, is the energetically most favorable pathway (see Figure 1). Furthermore, the initially formed cyclopropenylidene, in addition to decaying via a barrierless channel to c-$C_3H + H$, can also isomerize either to vinylidenecarbene (H_2CCC) via H migration/ring opening or to propargylene (HCCCH) through ring opening. Through a barrierless H-loss process, both H_2-CCC and HCCCH can, in turn, lead to l-$C_3H + H$ and via H_2 elimination to $C_3 + H_2$ via an exit potential barrier, as found in dynamical[26] and statistical[32] calculations.

Because the initially formed c-C_3H_2 resides in a very deep potential well (it is the most stable C_3H_2 isomer; see Figure 1), it is reasonable to expect at least an osculating complex mechanism for the reactions leading to either $C_3H + H$ or $C_3 + H_2$ formation. Indeed, our work finds that the $T(\theta)$'s for the two pathways have similar trends (see Figure 10), consistent with an osculating complex mechanism at $E_c = 49.1$ kJ mol^{-1}. In the work of Kaiser et al.,[27] the strongly forward-peaked $T(\theta)$ at $E_c = 45$ kJ mol^{-1} was interpreted as evidence of direct scattering dynamics via a very short-lived c-C_3H_2 intermediate (sub-picosecond lifetime) leading to a nonstatistical energy partitioning. This interpretation was considered to be supported by the nondetection of the $C_3 + H_2$ channel. It was argued that the reaction time scale is too short for a H-atom migration from c-C_3H_2 to either H_2CCC or HCCCH, which therefore were not involved in the reaction. Admittedly, Kaiser et al.[27] speculated that at low E_c, the c-C_3H_2 lifetime should have been long enough to permit energy randomization, and therefore, H migration to HCCCH and/or H_2CCC could have been possible, leading to the observation of both H- and H_2-elimination channels (c/l-C_3H and C_3 formation). Our study demonstrates that this is actually occurring also at the relatively high E_c of 49.1 kJ mol^{-1}.

Although the branching ratio $C_3/(C_3 + C_3H)$ as a function of E_c cannot be estimated reliably for the $C(^1D)$ reaction, we have an indication that at $E_c = 49.1$ kJ mol^{-1}, it is comparable to that of the $C(^3P)$ reaction. Bowman and co-workers[26] have found in preliminary calculations that singlet C_3H_2 produces c-C_3H, l-C_3H, and C_3 in comparable amounts. Statistical calculations by Mebel[50] indicate that at high E_c (about 50 kJ mol^{-1}), although the formation of l-$C_3H + H$ is the most important decay channel, the formation of c-$C_3H + H$ and C_3+H_2 (in comparable amounts) is still significant. Dynamical calculations on an accurate PES are desirable.

V. Astrophysical Implications

This work may have important implications for the chemistry of the interstellar medium. The present data, together with those presented previously,[19] have permitted us to draw a clearer picture of the distinct dynamics of c-C_3H and l-C_3H formation from the $C(^3P) + C_2H_2$ reaction. The estimation of the $\sigma_{cyclic}/\sigma_{linear}$ ratio now covers a very wide range of E_c's (from 0.8 up to 49.1 kJ mol^{-1}, corresponding to a temperature range of about 65−3500 K) and is found to decrease as E_c (temperature) increases, from ∼9 at 0.8 kJ mol^{-1} to 1 at 49.1 kJ mol^{-1}. Notably, the values obtained at $E_c = 0.8$ and 3.6 kJ mol^{-1} are close to the relative density of c-C_3H and l-C_3H observed in dense cloud TMC-1 (see ref 16).[5,6]

The current investigation of the dynamics of the spin-forbidden $C_3 + H_2$ reaction pathway has made it possible to estimate the $C_3/(C_3 + C_3H)$ branching ratio as a function of collision energy from 3.6 to 49.1 kJ mol^{-1}. It has been found that the branching ratio increases when the energy decreases and that C_3 and C_3H are formed in comparable amounts at $E_c = 3.6$ kJ mol^{-1}, equivalent to $T = 300$ K (see Figure 12). Although caution should be used when extrapolating the CMB data to the low translational energies (temperatures) typical of cold molecular clouds, from the trend shown in Figure 12, one

may reasonably expect a branching ratio of ~0.5−0.6 at very low temperatures. C_3 detection has been successful toward the Sgr B2 molecular cloud and carbon rich star IRC+10216.[9] In conclusion, the message of this work is that because of the strong energy (temperature) dependence of the cross sections (rate constants) for C_3H isomers and C_3 product formation, the collision energy and temperature-dependent branching ratios for particular products need to be included in chemical reaction networks modeling the abundances of cold molecular clouds.[51]

The above information on the three competing pathways of the title reaction may also be useful in the modeling of combustion processes and circumstellar envelopes of dying carbon stars, where temperatures approach those of combustion environments. Finally, the information gathered on the $C(^1D) + C_2H_2$ reaction may be useful for understanding the chemistry of comets because of the high production rate of $C(^1D)$ in these objects (where photoionization of CO, followed by dissociative recombination with electrons, is thought to be the main source of $C(^1D)$). Notably, both C_3H and C_3 have been observed in comets,[52] and the reaction of excited carbon atoms with acetylene may well be, at least in part, the source of these observed species. Prospective reaction networks of cometary chemistry must consider C_3 products as well as (possibly) distinct C_3H product isomers.

VI. Summary and Conclusions

We have reported a detailed investigation of the dynamics of the reactions of ground- and excited-state carbon atoms, $C(^3P)$ and $C(^1D)$, with acetylene over a wide collision energy range (3.6−49.1 kJ mol^{-1}) using the CMB scattering technique with electron ionization mass spectrometric detection and time-of-flight analysis. From angular and TOF distribution measurements of products at $m/z = 37$ and 36, the primary reaction products of both the $C(^3P)$ and $C(^1D)$ reactions with C_2H_2 have been identified to be c-C_3H + H, l-C_3H + H, and $C_3 + H_2$. Product angular and translational energy distributions in the CM system for the l- and c-C_3H isomers as well as the C_3 product from the $C(^3P)$ and $C(^1D)$ reactants have been derived as a function of collision energy. In the case of the $C(^3P)$ reaction, it has been possible to characterize the distinct dynamics of the two different C_3H isomers, while in the case of the $C(^1D)$ reaction, this was not possible.

Formation of both C_3H isomers is possible following the initial attack of $C(^3P)$ onto the unsaturated bond of acetylene; triplet cyclopropenylidene can give the cyclic isomer by CH bond cleavage, while propargylene (and, to a much smaller extent, vinylidenecarbene) can give the linear one (see Figure 1). While the lifetime of propargylene is calculated to be very long (up to microseconds) even at high temperatures (E_c's)[32] (see Table 4), correlating very well with the symmetric $T(\theta)$ observed for l-C_3H (Figure 7) and a long-lived complex reaction mechanism, the lifetime of triplet cyclopropenylidene is considerably shorter[32] (see Table 4) but still long enough at low E_c with respect to its rotational period to justify the interpretation of the reaction mechanism in terms of a long-lived complex mechanism for c-C_3H formation.

The ratios of cross sections σ(c-C_3H)/σ(l-C_3H) and the branching ratio $\sigma_{C_3}/(\sigma_{C_3} + \sigma_{C_3H})$ from the $C(^3P)$ reaction have been determined, and both have been found to increase with decreasing E_c. Formation of the spin-forbidden $C_3(X^1\Sigma_g^+)$ + H_2 products from the $C(^3P)$ reaction has been rationalized in terms of ISC between triplet and singlet C_3H_2 potential energy surfaces. The overall results have been discussed in light of the available theoretical information on the relevant triplet and singlet C_3H_2 ab initio potential energy surfaces. The exoergicity of 11 ± 2 kJ mol^{-1} determined in our previous work[19] and confirmed here is corroborated by the new accurate theoretical value of Mebel et al.[32] of 14.1 ± 4 kJ mol^{-1}. Comparisons have been made with the available theoretical predictions (approximate quantum scattering calculations and quasiclassical trajectory calculations on the triplet PES without nonadiabatic effects and statistical calculations including nonadiabatic effects) and with the results of previous crossed molecular beam studies using pulsed beams. The c-C_3H/l-C_3H ratio of cross sections from the $C(^3P)$ reaction as a function of E_c is found to be in rather good agreement with the results of very recent statistical calculations on ab initio potential surfaces (with and without inclusion of ISC), while it differs strongly from the results of the dynamical calculations on different ab initio triplet PESs. The statistical calculations corroborate also the trend with E_c of the experimental branching ratio $\sigma_{C_3}/(\sigma_{C_3} + \sigma_{C_3H})$ from the $C(^3P)$ reaction, although they appear to underestimate somewhat the extent of ISC. This could be due to inaccuracies in the PESs (nonadiabatic coupling elements, for instance) or to dynamical effects, or to both. Again, QCT calculations on accurate triplet/singlet ab initio PESs including nonadiabatic effects are desirable. The CM angular distribution of c-C_3H is found to be isotropic (backward−forward symmetric) at all E_c's, reflecting the formation of a long-lived cyclic C_3H_2 complex even at 50 kJ mol^{-1}; this is corroborated by statistical calculations of the theoretical lifetime as a function of E_c by Mebel et al.[32] The CM angular distribution of l-C_3H is found to be backward−forward symmetric at low E_c, reflecting the formation of a long-lived linear C_3H_2 complex, and becomes increasingly more forward scattered with increasing E_c, reflecting an osculating complex mechanism, as suggested by the statistical lifetime calculations. This trend (long-lived complex mechanism at low E_c and osculating complex mechanism at high E_c) is opposite to the trend derived from previous CMB experiments with pulsed beams, where a forward-scattered overall (that is, linear + cyclic) C_3H CM angular distribution was derived at low E_c (about 8 kJ mol^{-1}), which becomes progressively less forward scattered with increasing E_c, up to becoming backward−forward symmetric (isotropic) at $E_c = 45.2$ kJ mol^{-1} (only l-C_3H being formed at this high E_c). Significant differences are also noted in the trend of the C_3 product CM angular distributions with respect to that recently derived from pulsed CMB work. The interpretation of the reaction dynamics of $C(^3P) + C_2H_2$ derived in the present study consequently contradicts that obtained from the previous pulsed CMB studies of Kaiser et al.[12−14,20] Although the $C(^3P) + C_2H_2$ reaction appears to be nearly statistical, significant differences are noted between the experimental results and the statistical predictions. Dynamical calculations on more accurate PESs with inclusion of nonadiabatic effects are desirable for a more quantitative understanding of the detailed dynamics of this fundamental reaction.

The $C(^1D) + C_2H_2$ reaction is also found to lead to c/l-C_3H + H and $C_3 + H_2$. While for $C(^3P) + C_2H_2$ the $C_3 + H_2$ channel is spin forbidden, it is allowed for the $C(^1D)$ reaction. At low E_c, both H and H_2 elimination are found to proceed via a long-lived complex mechanism, while at high E_c, they both proceed via an osculating complex mechanism, reflecting a lifetime of the singlet intermediate from the $C(^1D)$ asymptote which is comparable or shorter than its rotational period. Finally, the astrophysical implications of the present results have been discussed.

Acknowledgment. We acknowledge financial support from the Italian MIUR (Ministero Istruzione Università Ricerca) under

Projects PRIN 2003 and 2005 and FIRB 2001. This work is also supported by the European Union Marie-Curie human resources and mobility programme, including a postdoctoral fellowship for K.M.H., under Contract MCRTN-CT-2004-512302, Molecular Universe. We thank A. M. Mebel for stimulating and useful correspondence and generous sharing unpublished results. P.C. wishes to acknowledge the Dalian Institute of Chemical Physics (DICP)-Chinese Academy of Sciences (CAS) for a visiting professorship and Xueming Yang for his hospitality at the State Key Laboratory for Molecular Reaction Dynamics (SKLMRD), DICP-CAS, Dalian, China, where the writing of this paper was completed. Finally, it is a great pleasure to dedicate this paper to Professor Giacinto Scoles on the occasion of his 72nd birthday. Giacinto Scoles has been a pioneer in scattering experiments and continues to be an example and inspiration to many of us.

References and Notes

(1) Ochsenfeld, C.; Kaiser, R. I.; Lee, Y. T.; Suits, A. G.; Head-Gordon, M. *J. Chem. Phys.* **1997**, *106*, 4141

(2) Lis, D. C.; Blake, G. A.; Herbst, E. *Astrochemistry: Recent Successes and Current Challenges*; Cambridge University Press: New York, 2006.

(3) *Faraday Discuss.* **2001**, *119*, Combustion Chemistry: Elementary Reactions to Macroscopic Processes.

(4) Frenklach, *Phys. Chem. Chem. Phys.* **2002**, *4*, 2028.

(5) Turner, B. E.; Herbst, E.; Terzevia, R. *Astrophys. J. Suppl. Ser.* **2000**, *126*, 427.

(6) Fossé, D.; Cernicharo, J.; Gerin, M.; Cox, P. *Astrophys. J.* **2001**, *552*, 168.

(7) Hinkle, K. W.; Keady, J. J.; Bernath, P. F. *Science* **1988**, *241*, 1319.

(8) Bernarth, P. F. Laboratory Astrophysics and Molecular Astronomy of Pure Carbon Molecules. In *Life Sciences and Space Research XXV (4)*; Pergamon Press Ltd: Oxford, U.K., 1994; Vol. 15, p 15.

(9) Cernicharo, J.; Goicoechea, J. R.; Caux, E. *Astrophys. J.* **2000**, *534*, L199.

(10) (a) Haider, N.; Husain, D. *Z. Phys. Chem.* **1992**, *176*, 133. (b) Clary, D. C.; Haider, N.; Husain, D.; Kabir, M. *Astrophys. J.* **1994**, *422*, 416.

(11) (a) Chastaing, D.; James, P. L.; Sims, I. R.; Smith, I. W. M. *Phys. Chem. Chem. Phys.* **1999**, *1*, 2247. (b) Chastaing, D.; Le Picard, S. D.; Sims, I. R.; Smith, I. W. M. *Astron. Astrophys.* **2001**, *365*, 241.

(12) Kaiser, R. I.; Ochsenfeld, C.; Head-Gordon, M.; Lee, Y. T.; Suits, A. G. *J. Chem. Phys.* **1997**, *106*, 1729.

(13) Kaiser, R. I.; Ochsenfeld, C.; Head-Gordon, M.; Lee, Y. T.; Suits, A. G. *Science* **1996**, *274*, 1508.

(14) Kaiser, R. I.; Stranges, D.; Lee, Y. T.; Suits, A. G. *Astrophys. J.* **1997**, *477*, 982.

(15) Geppert, W. D.; Naulin, C.; Costes, M. *Chem. Phys. Lett.* **2001**, *333*, 51.

(16) Casavecchia, P.; Balucani, N.; Cartechini, L.; Capozza, G.; Bergeat, A.; Volpi, G. G. *Faraday Discuss.* **2001**, *119*, 27.

(17) Cartechini, L.; Bergeat, A.; Capozza, G.; Casavecchia, P.; Volpi, G. G.; Geppert, W. D.; Naulin, C.; Costes, M. *J. Chem. Phys.* **2002**, *116*, 5603.

(18) Clary, D. C.; Buonomo, E.; Sims, I. R.; Smith, I. W. M.; Geppert, W. D.; Naulin, C.; Costes, M.; Cartechini, L.; Casavecchia, P. *J. Phys. Chem. A* **2002**, *106*, 5541.

(19) Costes, M.; Daugey, N.; Naulin, C.; Bergeat, A.; Leonori, F.; Segoloni, E.; Petrucci, R.; Balucani, N.; Casavecchia, P. *Faraday Discuss.* **2006**, *133*, 157.

(20) Guo, Y.; Mebel, A. M.; Gu, X.; Kaiser, R. I. *J. Phys. Chem.* A **2007**, *111*, 2980.

(21) Takahashi, J.; Yashimata, K. *J. Chem. Phys.* **1996**, *104*, 6613.

(22) Guadagnini, R.; Schatz, G. C.; Walch, S. P. *J. Phys. Chem. A* **1998**, *102*, 5857.

(23) Mebel, A. M.; Jackson, W. M.; Chang, A. H. H.; Lin, S. H. *J. Am. Chem. Soc.* **1998**, *120*, 5751.

(24) Buonomo, E.; Clary, D. C. *J. Phys. Chem. A* **2001**, *105*, 2694.

(25) (a) Takayanagi, T. *Chem. Phys.* **2005**, *312*, 61. (b) Takayanagi, T. *J. Phys. Chem. A* **2006**, *110*, 361.

(26) Park, W. K.; Park, J.; Park, S. C.; Braams, B. J.; Chen, C.; Bowman, J. M. *J. Chem. Phys.* **2006**, *125*, 081101.

(27) Kaiser, R. I.; Mebel, A. M.; Lee, Y. T. *J. Chem. Phys.* **2001**, *114*, 231.

(28) Bergeat, A.; Cartechini, L.; Casavecchia, P.; Volpi, G. G. Proceedings of the 25th International Symposium on Free Radicals, Flagstaff, AZ, August 15−20, 1999; p 42.

(29) (a) Fisk, G. A.; Mc Donald, J. D.; Herschbach, D. R. *Discuss. Faraday Soc.* **1967**, *44*, 28. (b) Miller, W. B.; Safron, S. A.; Herschbach, D. R. *Discuss. Faraday Soc.* **1967**, *44*, 108. (c) Miller, W. B.; Safron, S. A.; Herschbach, D. R. *J. Chem. Phys.* **1972**, *56*, 3581. See also: Liu, K. *J. Chem. Phys.* **2006**, *125*, 132307.

(30) Bergeat, A.; Loison, J.-C. *Phys. Chem. Chem. Phys.* **2001**, *3*, 2038.

(31) Kaiser, R. I.; Le, T. N.; Nguyen, T. L.; Mebel, A. M.; Balucani, N.; Lee, Y. T.; Stahl, F.; Schleyer, P. v. R.; Shaefer, H. F., III. *Faraday Discuss.* **2001**, *119*, 51.

(32) Mebel, A. M.; Kislov, V. V.; Hayashi, M. *J. Chem. Phys.* **2007**, *126*, 204310.

(33) At the higher E_c of 18.5 kJ mol^{-1}, the C_3 $T(\theta)$ reported in ref 16 was very slightly forward biased; however, a reanalysis of the best fit using an improved calibration of the velocity of both beams (the refined E_c is 18.6 kJ mol^{-1}, and the CM angle is unchanged) indicates that the $T(\theta)$ of C_3 is actually isotropic within the error bars. Additionally, a recalibration of the velocity of both beams for the previous data at $E_c = 3.5$ kJ mol^{-1} left also unchanged the CM angle while it increased slightly the most probable E_c from 3.5 to 3.6 kJ mol^{-1}, referred to in the previous[19] and present paper as 3.5 and 3.6 kJ mol^{-1}, respectively).

(34) Alagia, M.; Balucani, N.; Casavecchia, P.; Stranges, D.; Volpi, G. G. *J. Chem. Soc., Faraday Trans.* **1995**, *91*, 575.

(35) Casavecchia, P. *Rep. Prog. Phys.* **2000**, *63*, 355.

(36) Casavecchia, P.; Capozza, G.; Segoloni, E. In *Modern Trends in Chemical Reaction Dynamics, Experiment and Theory (Part II)*; Yang, X., Liu, K., Eds.; Advanced Series in Physical Chemistry, Vol. 14; World Scientific: Singapore, 2004; Chapter 7.

(37) Capozza, G.; Segoloni, E.; Leonori, F.; Volpi, G. G.; Casavecchia, P. *J. Chem. Phys.* **2004**, *120*, 4557.

(38) Casavecchia, P.; Capozza, G.; Segoloni, E.; Leonori, F.; Balucani, N.; Volpi, G. G. *J. Phys. Chem. A* **2005**, *109*, 3527.

(39) Balucani, N.; Capozza, G.; Leonori, F.; Segoloni, E.; Casavecchia, P. *Int. Rev. Phys. Chem.* **2006**, *25*, 109.

(40) Sköld, K. *Nucl. Instrum. Methods* **1968**, *63*, 114.

(41) Bergeat, A.; Cartechini, L.; Balucani, N.; Capozza, G.; Phillips, L. F.; Casavecchia, P.; Volpi, G. G.; Bonnet, L.; Rayez, J.-C. *Chem. Phys. Lett.* **2000**, *327*, 197.

(42) Balucani, N.; Capozza, G.; Cartechini, L.; Bergeat, A.; Bobbenkamp, R.; Casavecchia, P.; Aoiz, F. J.; Bañares, L.; Honvault, P.; Bussery-Honvault, B.; Launay, J.-M. *Phys. Chem. Chem. Phys.* **2004**, *6*, 4957.

(43) Balucani, N.; Capozza, G.; Segoloni, E.; Russo, A.; Bobbenkamp, R.; Casavecchia, P.; Gonzalez-Lezana, T.; Rackham, E. J.; Bañares, L.; Aoiz, F. J. *J. Chem. Phys.* **2005**, *122*, 234309.

(44) Gu, X.; Guo, Y.; Mebel, A. M.; Kaiser, R. I. *J. Phys. Chem.* A **2006**, *110*, 11265.

(45) (a) Casavecchia, P. *Faraday Discuss.* **2006**, *133*, 356. (b) Leonori, F.; Petrucci, R.; Segoloni, E.; Balucani, N.; Hickson, K.; Le Picard, S.; Foggi, P.; Casavecchia, P. *Planet. Space Sci.* Submitted.

(46) Lee, Y. T. In *Atomic and Molecular Beam Methods*; Scoles, G., Ed.; Oxford University Press: New York, 1987; Vol. 1, pp 553−568.

(47) (a) Levine, R. D.; Bernstein, R. B. *Molecular Reaction Dynamics and Chemical Reactivity*; Oxford University Press: New York, 1987. (b) Levine, R. D. *Molecular Reaction Dynamics*; Cambridge University Press: New York, 2005.

(48) Okabe, H. *Photochemistry of Small Molecules*; Wiley: New York, 1978.

(49) Gingerich, K. A.; Finkbeiner, H. C.; Schmude, R. W. *J. Am. Chem. Soc.* **1994**, *116*, 3884.

(50) Mebel, A. M. Personal communication.

(51) (a) Herbst, E. *Annu. Rev. Phys. Chem.* **1995**, *46*, 27. (b) Herbst, E. *J. Phys. Chem. A* **2005**, *109*, 4017.

(52) Gausset, L.; Herzberg, G.; Lagerqvist, A.; Rosen, B. *Astrophys. J.* **1965**, *142*, 45.